BC hydro

Peace River Project Water Use Plan

Title: A Feasibility Study for the Development of a RADARSAT-2 Dust Prediction System

Reference GMSWORKS-20

Implementation Year 3

A Feasibility Study for the Development of a RADARSAT-2 Dust Prediction System: 2011 Annual Report

Study Period: January 1, 2011 – February 17, 2012

Dr. W.G. Nickling,
Dr. J. A. Gillies and
Dr. L. Brown

Nickling Environmental Ltd
Cambridge, Ontario

July 18, 2012

TABLE OF CONTENTS

EXECUTIVE SUMMARY

In the spring of 2009 a project was initiated to assess the feasibility of developing a model to identify the dust emission potential of beaches around the Williston Reservoir in relation to textural, surficial and meteorological conditions. A model of this nature can form the basis of an operational plan on when and where to apply dust control measures to maximize the investment on reducing the PM_{10} concentrations that impact the local and regional environment, while saving costs related to mitigation efforts. In order to develop strategies and inform management decisions to reduce PM_{10} dust emissions from Williston Reservoir beaches it is necessary to develop an understanding of the dust emission potential for the beaches including the strength of the emissions and how they vary as a function of location and through time. A strategy to evaluate emission potential for the beaches uses the Portable In-Situ Wind Erosion Laboratory (PI-SWERL) to estimate the critical wind shear velocity that initiates the movement of sand and the emission of dust (u_{*t}, m s^{-1}). Wind shear velocity (u_*, m s^{-1}) is the critical atmospheric parameter that drives wind erosion and dust emission. PI-SWERL is also used to directly measure the relationship between dust flux (F, µg m^{-2} s^{-1}) and u_*, m s^{-1}. PI-SWERL applies a known shear velocity to the beach surface and based on measurements of PM_{10} concentration and volumetric flow through the instrument estimates F. Application of multiple shear velocities allows for the development of a beach-specific emission potential relationship. Along with PI-SWERL measurements, samples of the beach sediments are collected for soil texture (i.e., quantification of % sand, % silt, and % clay composition) and moisture content (ratio of H_2O mass : sediment mass).

To date three years of PI-SWERL, sediment texture, and moisture content measurements have been collected at the Williston Reservoir for 18 different beaches. In 2011, measurements of soil texture indicate that there are year-to-year variation in the relative proportions of sand, silt, and clay. The change in texture will affect dust emissions potential.

The data from 2011 for u_{*t} for PM_{10} emissions indicate that it increased on average 32% (±19%) between 2010 and 2011. There is not such a clear trend for the threshold of the sand-sized particles. As the range of moisture content of the sediments was very similar between 2010 and 2011, it suggests that relative humidity may have played a key role. The cooler and wetter (higher precipitation and relative humidity) conditions that prevailed in 2011 likely caused the increase u_{*t}. The effect of RH on u_{*t} reaches a well-defined maximum at RH≈35%.

PM_{10} emissions also changed between 2010 and 2011 for beaches measured in both years. In all cases the PM_{10} flux (µg m^{-2} s^{-1}) measured in 2011 for the second and third applied shear stresses (i.e., u_*=0.31 m s^{-1} and u_*=0.46 m s^{-1}) were significantly less than the mean values measured in 2010. For the beaches with three years of data, i.e., Davis and Collins, the PM

emission potentials are more similar to those measured in 2009. Two reasons can be advanced as to what caused the reduction of emission potential in 2011 compared with 2010. The first is that the cooler and moister conditions (i.e., higher RH) that prevailed in 2011 reduced emissions and second there was a decrease in clay content of the beaches between these years. The clay content is the critical reservoir of the PM_{10} component of the sediments. Of note, even though PM_{10} emission potential was in general lower in 2011 than 2010, is that four of the same beaches were identified as being the highest emitters in both years. These beaches are: Middle Creek North, Tsay Keh, Davis North, and Shovel. It is recommended that these beaches be considered a high priority for management to reduce PM_{10} emissions.

The overall modelling goal of the 2011 season was to enhance the data sets of 2009 and 2010 to identify the locations, textural characteristics, associated threshold wind speed and potential emissions from "hot spots" where a large percentage of the total atmospheric dust loading may originate. The 2011 PI-SWERL measurements of u_{*t}, and F α u_*, along with the surface soil texture, serve as input for the WE_DUST_EM model. The wind speeds during the May 20 to June 20 modelling period are used to calculate the potential dust emissions as a function of location for the Williston Reservoir beaches. The subsequent model output once mapped shows the spatial distribution of dust emissions.

Based on the 2011 input data the WE_DUST_EM model predicted much lower daily dust emissions than those of 2010. This can, in part, be attributed to the lack of wind storms in 2011, whereas in 2010 these storms resulted in high wind speeds that persisted throughout the day. It was on these windy days that WE_DUST_EM successfully predicted days of high emissions that corresponded to the dates where dust storms occurred in the valley as measured by dust sampling instrumentation deployed as part of the Tillage Trials and Regional Air Monitoring programs (Nickling et al. 2011). Results of this year's modelling efforts affirm there is a spatial distribution to dust emissions on the reservoir beaches and the high emission beaches are found in the Collins, Davis, Shovel and Middle Creek locations. However, the winds of the 2011 season do not generate dust emission from the bottom section of the study area that was active in the 2010 season. Further repeated PI-SWERL testing of the 2009, 2010 and 2011 sites is needed to confirm whether these emitting sites remain stable through time. This will provide valuable information to inform mitigation strategies, for example if they should be focused in the same areas every dust emission season to more efficiently reduce the overall dust emission burden at the reservoir and the effect of this dust on air quality at the Tsay Keh village.

The 2011 study further confirms the efficacy of the PI-SWERL as a cost effective instrument for the measurement of both threshold shear velocity for the onset of wind erosion and dust emission and develop the relationship between shear velocity and dust flux for sites with great economy of labour and logistics, as compared with more traditional methods such as tower-

based or large portable wind tunnel measurements. However, the measurements quantify dust emissions for specific points on the beaches to quantify dust emission patterns over the entire study area a dust emission model must be used. Therefore, to fully predict dust emission from the Williston Reservoir beaches PI-SWERL testing to constrain the temporal and spatial variability of potential emissions coupled with the WE_DUST_EM model provides a feasible PM_{10} emission prediction system. Use of this system to build a more complete data set of beach emissions can be used as a management tool to guide the dust control measures that will reduce the impacts of these emissions on the local and regional air quality.

1.0 INTRODUCTION

Each year the draw-down of the Williston Reservoir for the production of hydro electric power exposes several thousand hectares of wide flat beaches comprised predominantly of relatively fine grained sediments. These sediments are very prone to deflation by wind resulting in large dust storms that may affect human health and the quality of life for inhabitants of the valley. Various control measures have been proposed to reduce dust emissions (e.g., tillage, water sprays, planting of vegetation and development of wetlands), several of which are currently being assessed for implementation. Despite this on-going work on mitigation techniques, no effective methodology or strategy is currently available to delineate the location and areal extent of those beaches that are most likely to erode at any given time. Knowledge of the likelihood of an erosion and dust emission event is desirable so that a given control method (e.g., tillage or water spray) can be implemented at the right location in a timely manner to allow preventive measures to be undertaken to reduce or eliminate dust emissions. This approach can result in reduced control costs by applying appropriate mitigation measures to only those areas that have the greatest potential to erode and release dust. Although no predictive model of this nature currently exists, remote sensing and field techniques as well as modeling approaches are available that can be used to guide the development of an effective methodology and predictive wind erosion model for the Williston Reservoir.

In 2009 a project was initiated with the goal to evaluate the feasibility of using RADARSAT-2 as a means to acquire data on the emission condition of Williston Reservoir beaches that could be used in the development of a dust emission model. Although good progress was made towards the development of the dust emission model, RADARSAT-2 was found to be too costly and difficult to manipulate for this particular application. As a result a different approach using LANDSAT imagery was adopted. As part of this feasibility study, potential dust emissions, which provide necessary input for the model, were evaluated at selected beaches on the Williston Reservoir using the Portable In-Situ Wind Erosion Lab PI-SWERL) (Etyemezian et al., 2007). This instrument is being used increasingly as a primary tool to evaluate windblown dust emissions from natural and artificial soil surfaces because of its ease of operation and cost effectiveness

when compared to larger, more logistically challenging, portable field wind tunnels. As a result of the success of these preliminary investigations, an intensive study was undertaken in 2010 to obtain additional data on the potential emission of particles less than or equal to 10 μm aerodynamic diameter (i.e., PM_{10}), for beaches that surround the Williston Reservoir using the PI-SWERL In addition to the PI-SWERL measurements, data on the grain size of the beach sediments and their moisture content at the time of testing were collected. These two characteristics of the sediments can critically affect the wind speed needed to mobilize the sediments as well as the strength of the dust emissions. In order to extend the range and general applicability of the dust prediction model, it was deemed necessary to carry out additional PI-SWERL testing on additional beaches as well as some of the same beaches tested in 2010, in spring 2011.

1.1 Study Goals and Objectives

The overall goal of this study was to extend the range and general applicability of the dust prediction model that was developed as part of the study by Nickling et al. (2010) and to enhance the data set of 2009 by characterizing a greater spatial extent of Williston beach environments, examining temporal variability of the threshold wind speed at which dust emissions begin, and the strength of those emissions as a function of wind speed. These new data are to be used to better-define the relationships between these parameters and surface moisture content and textural conditions, and link these measurements to specific geographic locations. A knowledge of emission potential as a function of location can serve as a powerful guide for directing dust mitigation operations.

To achieve the above stated goal, two major objectives were developed for the 2010 field study and carried forward to the 2011 study:

1) Quantify the range of potential dust emissions at beaches throughout the reservoir to the best of our ability to meet the challenges of weather, travel restrictions, and other logistical constraints.

2) Identify the locations, textural characteristics, associated threshold wind speed and potential emissions from “hot spots” where a large percentage of the total atmospheric dust loading may originate.

2.0 Measuring Dust Entrainment Thresholds and Emission Fluxes

Critical parameters for evaluating the dust emission characteristics of a susceptible surface include the wind speed, or more correctly the wind shear stress (τ, N m^{-2}) or wind shear velocity (u_*, m s^{-1}, note $\tau = \rho\, u_*^2$ where ρ is air density, kg m^{-3}) that causes the sediments to be entrained into the wind (i.e., the threshold for entrainment), as well as the strength of those

dust emissions (i.e., emission rate, F, µg m^{-2} s^{-1}) in relation to the magnitude of the shearing stress. Particle emission thresholds are critically controlled by: particle size of the sediments, moisture content, soil texture (i.e., percent sand, silt, and clay), and surface roughness. It is generally accepted that the dust emission scales as power function of the wind shear stress (e.g., Shao 2000), with recent theoretical evaluations (e.g., Shao 2004) supporting a third power relationship (i.e., $F \propto a\, u_*^3$), but a wide range of exponent values have been observed (Gillies, 2012).

2.1 Measurement Program

Following directly from the successful measurement campaign of 2009 and 2010 that used the PI-SWERL, this instrument was utilized again in 2011. The PI-SWERL is highly portable, operated by one to two people, and economical for field measurements with a typical test completed in less than 20 minutes. Direct comparisons of PI-SWERL measurements with the University of Guelph, straight-line field wind tunnel at seventeen sites in the Mojave Desert (Sweeney et al. 2008) showed very good correspondence between the two measurement methods.

2.2 Site Selection

In spring 2011, beaches for sampling were selected based on knowledge gained from the study of Nickling et al. (2010), as well as observations made by the field team in 2009, and in consultation with other personnel working at the reservoir who have traversed much of the reservoir beaches carrying out various activities (e.g., tilling operations, archeological work, project management, etc.).

The sampling locations were selected, as much as possible to capture the diversity of soil characteristics of the beaches surrounding the reservoir and their associated dust emission potential. A constraint on the sampling program was travel restrictions in that the beaches had to be accessible to all-terrain vehicles (i.e., a Ranger), which was especially relevant for the transportation of the PI-SWERL. PI-SWERL was transported to the beaches by a Ranger. A list of the test locations where PI-SWERL and surface characterization data were collected are presented in Table 2.1.

Table 2.1. The date, time, and location of the PI-SWERL transects carried out in 2011.

Date	Location	Transect	Time		# of tests
			Start	End	
19-May	Collins	3	10:55	12:22	10
	Collins	2	13:19	14:49	10
	Collins	5	15:12	16:48	10
20-May	Collins	3	9:52	11:31	10
	Collins	1	12:12	13:36	10
21-May	Davis N	2	10:38	12:08	9

	Davis N	1	12:45	14:08	10
25-May	Davis N	3	10:57	12:25	10
	Davis N	4	12:45	14:38	10
	Davis N	5	15:02	16:47	11
26-May	Davis N	6	11:22	12:05	5
	Davis N	7	12:25	13:15	5
27-May	Davis S	1	10:27	11:52	10
	Davis S	2	12:11	13:31	10
	Davis S	3	13:54	14:35	5
29-May	Middle Creek N	1	10:34	12:16	10
	Middle Creek N	2	12:25	13:40	10
30-May	Middle Creek N	3	10:26	11:48	10
	Middle Creek N	4	12:02	13:23	10
	Middle Creek N	5	13:39	14:59	9
31-May	Middle Creek S	1	10:51	12:10	10
	Middle Creek S	2	12:27	13:56	10
01-Jun	Shovel	1	11:09	12:30	10
	Shovel	2	12:40	14:27	10
	Shovel	3	14:40	15:17	5
02-Jun	Middle Creek S	3	11:11	12:38	10
	Middle Creek S	4	12:53	14:19	10
	Middle Creek S	5	2:47	15:25	5
06-Jun	Shovel	4	11:48	13:09	10
	Shovel	5	13:23	14:27	10
07-Jun	Corless A	1	10:19	11:42	10
	Corless A	2	11:57	1:20	10
	Corless B	1	1:53	3:19	10
08-Jun	Tsay Keh	1	12:31	13:57	11
	Tsay Keh	2	14:07	16:28	10
09-Jun	Lafferty	1	10:56	12:21	10
	Lafferty	2	12:40	14:18	10
16-Jun	Lafferty	3	10:24	12:05	9
	Davis N	8	14:24	16:02	10
	Davis N	9	16:26	18:04	10
17-Jun	Von Somer	1	11:30	13:00	9
	Von Somer	2	13:13	14:02	5
	Tsay Keh	3	15:38	17:15	10
19-Jun	Ospika	1	11:44	12:41	5

2.3 Sampling Site Characteristics

In 2011, 12 beach areas were visited for to acquire measurements of potential dust emissions using the PI-SWERL. Brief descriptions of the characteristics found at each test site are provided in Table 2.2 along with a photograph of the area in which the PI-SWERL tests were undertaken.

Table 2.2. Descriptions of the PI-SWERL test sites, 2011.

(A) Collins 56°25.504', 124°24.742'

Located on the east shore. Sandy loam, easy to access, extensive area, heterogeneous composition. Lots of coarse woody debris towards the water as well

as the south region of the beach. Moderate emissivity.

(B) Corless A **56°26.361', 124°30.316'**

Located on the west shore, this beach is the Lorimer Regional Monitoring site. This sandy beach maintains evidence of previous tillage. Low emissivity.

(C) Corless B **56°26.000', 124°30.014'**

Located on the west shore, just south of Corless A. This beach is very similar in soil texture to Corless A (very sandy) but has many remaining tree trunks that may prohibit future tillage. Moderate emissivity.

(D) Davis N **56°32.753', 124°30.918'**

Located on the east shore, site of previous tillage and vegetation trial. The majority of this beach is Loamy sand, with some regions having a high silt and clay content.

extensive area, site of tillage and vegetation trials. Moderate to high emissivity.

(E) Davis S **56°31.325', 124°30.307'**

Located on the east shore, accessible by road at Fort Graham. Mostly medium sand, similar to Davis N. Lots of pebbles and coarse sand to the north, and some finer sediment to the south. Moderate emissivity.

(F) Lafferty **56°19.691', 124°29.212'**

Located on the east shore, south of Collins. Loamy sand, similar emission characteristics to Davis North. Significant coarse woody debris north of the Regional Monitoring site. Accessible by road and boat. Moderate to low emissivity.

(G) Middle Creek N **56°37.593', 124°37.927'**

Located on the east shore. Very homogeneous sand. Accessible by boat. High emissivity.

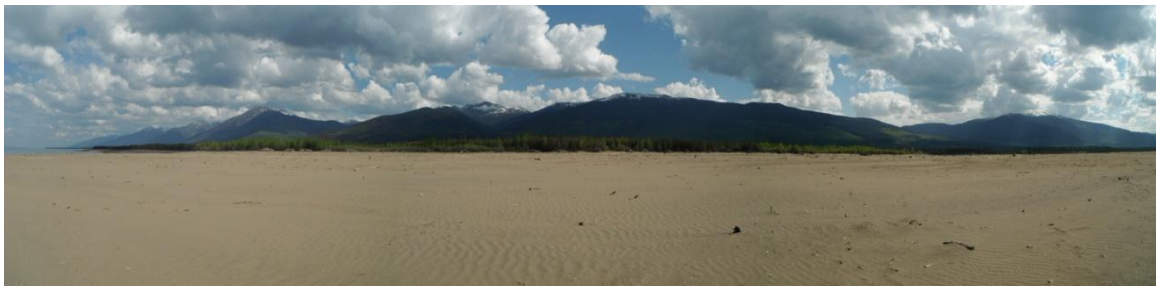

(H) Middle Creek S **56°37.426', 124°38.506'**

Located on the east shore. Mostly homogeneous sand, with great amount of visible emissions during storm events. Hardened silt and clay to the north, having a low emission potential. Significant amount of coarse woody debris to the south. Accessible by boat. High emissivity.

(I) Ospika **56°12.563', 124°08.865'**

Located on the east shore. Combination of sand and gravel with several regions of organic matter. Relatively high sediment transport threshold. Accessible by road. Low emissivity.

(J) Shovel **56°35.829', 124°25.298'**

Located on the east shore. Very homogeneous sand, similar in composition to Davis, Lafferty and Middle Creek N and S. Some isolated silt patches. Accessible by boat.

High emissivity.

(K) Tsay Keh **56°52.935', 124°57.865'**

Northernmost beach composed primarily of sand. Accessible by road from the village of Tsay Keh. High emissivity.

(L) Von Somer **56°49.215', 124°51.699'**

Located on the east shore, south of Ruby Red. Heterogeneous composition: dry, silty sand and regions with gravel. Low emissivity (no photo available).

2.4 PI-SWERL Test Results 2011

2.4.1 Sediment Texture of the Sampled Beach Areas

The textural characteristics of the sediment samples collected at each beach tested in 2009, 2010, and 2011 are shown in Table 2.3. The beach environments tested in both 2009 and 2010 were predominantly classified as sand (65%), 20% of the test beaches are classified as loamy sand, 10% are sandy loam, and 5% are silty clay loam. In 2011 the beaches tested with PI-SWERL were either sand (67% of tests) or loamy sand (33% of tests).

Table 2.3. The textural characteristics and soil type designations of the test areas from 2009, 2010, and 2011.

Location	Average % sand	Average % silt	Average % clay	Average soil class

Location	Average % sand	Average % silt	Average % clay	Average soil class
2009 Field Season				
Collins 1	88.2	4.5	7.3	loamy sand
Collins 2	89.8	3.8	6.4	sand
Collins 3	95.3	1.8	2.9	sand
Davis	94.3	3.3	2.4	sand
2010 Field Season				
Bevel	85.8	7.8	6.4	loamy sand
Bob Fry	3.4	58.5	38.1	silty clay loam
Collins	72.4	20.6	6.9	sandy loam
Corless (Lorimer)	95.9	1.4	2.7	sand
Corless (Stromquest)	95.9	1.5	2.6	sand
Davis North	84.6	10.9	4.5	loamy sand
Davis South	91.4	4.9	3.7	sand
Lafferty	76.5	17.3	6.2	loamy sand
Middle Creek N	92.4	2.1	5.5	sand
Middle Creek S	94.8	1.2	4.0	sand
Ospika	95.0	1.4	3.6	sand
Pete Toy	95.4	1.3	3.3	sand
Raspberry	95.8	1.4	2.8	sand
Ruby Red	69.4	25.4	5.2	sandy loam
Shovel	92.4	3.3	4.3	sand
Tsay Keh	89.0	6.5	4.5	sand
2011 Field Season				
Collins	86.2	11.3	2.5	sand
Corless A	95.8	3.9	0.3	sand
Corless B	97.9	1.6	0.4	sand
Davis N	71.9	22.9	5.2	loamy sand
Davis S	96.1	2.7	1.3	sand
Lafferty	74.9	21.1	3.9	loamy sand
Middle Creek N	95.3	3.6	1.0	sand
Middle Creek S	95.8	3.1	1.1	sand
Ospika	97.2	2.0	0.8	sand
Shovel	82.7	15.6	1.7	loamy sand
Tsay Keh	83.2	15.0	1.8	loamy sand
Von Somer	97.9	1.6	0.6	sand

Comparing the textural characteristics of sites that have been measured over the three years of the program indicates that individual sites do change from year to year. Two locations have

been measured for all three years, Collins and Davis South. Of these two sites, Davis South has the most stable texture with the percent sand varying on average 3%, silt 1.5%, and clay 1.6%, among the three years. Collins shows a much higher degree of change among the three years of measurements, with the average percent difference for sand being 12.4%, silt 11.5%, and clay 2.9%. In either case (Collins or Davis) the clay content is the most stable component however, this fraction contains the PM_{10} and $PM_{2.5}$ and small changes in clay content likely have a large effect on emission potential.

There are 10 sites to compare textural changes between 2010 and 2011 (Table 2.3). The percent difference of change between years for the same site indicate very large change especially for the silt and clay content ranging in absolute value terms from 22% to 371% for the silt component and 16% to 87% for the clay component. For the clay component the difference in clay content between 2010 and 2011, is that in all cases there was less clay content in 2011, i.e., the percent change was negative. The change in the sand component between years ranges from zero to 19%. It should be noted that the percent change values are more dramatic for the silt and clay components because of the delta change in much smaller values than the sand component. Nevertheless, these data indicate that the sediment texture of a beach does vary in both space and through time and cannot be treated as being static and unchanging. These data remain limited to three years and the differences may be more reflective of spatial variation than temporal variation as the points of measurement are not exactly the same from year to year. A longer period of measurements of soil texture would be required to evaluate the temporal variability of this soil property.

2.4.2 Particle Thresholds for Sand and Dust Entrainment

Entrainment threshold for the sand-sized particles and the emission of PM_{10} dust were determined from the particle count and PM_{10} concentration data obtained during the initial ramp period when the PI-SWERL blade accelerates from 0 to 1000 RPM. To define when (and at what magnitude of shear stress) transport begins we followed the same criteria used by Nickling et al., 2010).

The observed threshold shear velocity (u_{*t} m s^{-1}) values for sand movement (saltation) ranged from a minimum of 0.15 m s^{-1} for Collins, Davis N, and Tsay Keh to a maximum of 0.46 m s^{-1} for Collins and Von Somer. Using all the available u_{*t} data, the mean and standard deviation for each beach tested for all tests are shown in Tables 2.4 (sand) and 2.5 (dust). Lafferty beach has the lowest mean u_{*t} value for sand (0.20 m s^{-1} m s^{-1}) and Ospika the highest mean u_{*t} (0.34 m s^{-1}). The beaches with the lowest u_{*t} for PM_{10} dust emissions in 2011 were Davis N and Von Somer (0.17 m s^{-1}), for comparison the lowest mean u_{*t} in 2010 was Ruby Red (0.14 m s^{-1}). The beaches with the highest u_{*t} for PM_{10} dust was Collins and Lafferty (0.43 m s^{-1}). The highest mean u_{*t} for PM_{10} was Ospika with a mean of 0.39 m s^{-1}, which is similar to the mean value

estimated for this location for 2010 of 0.36 m s^{-1}. These threshold shear velocities are typical of those reported in the literature for sandy to sandy loam soils. The range of u_{*t} measured for sand movement (0.15 to 0.46 m s^{-1}) would be associated with 10 m wind speeds of 4.6 to 14.2 m s^{-1} (≈17 km $hr^{-1}$to ≈51 km hr^{-1}) assuming an average aerodynamic roughness length derived from the meteorological tower wind speed profiles on Davis beach in 2010.

As Figs. 2.1 and 2.2 show there is year to year variation in u_{*t} at the same locations. There is more variability in the dust emission threshold than the sand threshold. For all the beaches tested in 2010 and 2011 the measured mean values of u_{*t} for PM_{10} are higher in 2011. The average percent increase in u_{*t} values between the two years is 32% (±19%). Although speculative it seems likely that the cooler and wetter (higher precipitation and relative humidity) conditions that prevailed in 2011 resulted in the higher mean values of u_{*t}. It is well-known that increased moisture content and RH increase u_{*t} (McKenna Neuman and Nickling, 1989; Ravi et al., 2004; Ravi and d'Odorico, 2005). The effect of RH on u_{*t} reaches a well-defined maximum at RH≈35% (Ravi and d'Odorico, 2005).

Table 2.4. Mean threshold shear velocity (u*t) and associated standard deviation for sand on the tested beaches in 2011.

Location	# of tests	u_{*t} (m s^{-1}) Min.	u_{*t} (m s^{-1}) Max.	u_{*t} (m s^{-1}) Mean	Std. Dev. (m s^{-1})
Collins	50	0.15	0.46	0.31	0.08
Davis N	80	0.15	0.43	0.27	0.05
Davis S	25	0.23	0.23	0.23	0.03
Middle Creek N	49	0.23	0.35	0.29	0.02
Middle Creek S	45	0.24	0.34	0.28	0.02
Shovel	45	0.23	0.34	0.27	0.03
Corless A	20	0.25	0.37	0.28	0.03
Corless B	10	0.24	0.27	0.26	0.01
Tsay Keh	31	0.15	0.40	0.24	0.06
Lafferty	29	0.20	0.20	0.20	0.20
Von Somer	14	0.23	0.46	0.32	0.06
Ospika	5	0.31	0.36	0.34	0.02

Table 2.5. Mean threshold shear velocity (u*t) and associated standard for dust on the tested beaches in 2011.

Location	# of tests	u_{*t} (m s^{-1}) Min.	u_{*t} (m s^{-1}) Max.	u_{*t} (m s^{-1}) Mean	Std. Dev. (m s^{-1})
Collins	50	0.25	0.43	0.34	0.06
Davis N	80	0.17	0.39	0.28	0.04
Davis S	25	0.23	0.36	0.29	0.03

Middle Creek N	49	0.26	0.39	0.32	0.02
Middle Creek S	45	0.26	0.35	0.31	0.02
Shovel	45	0.20	0.36	0.29	0.03
Corless A	20	0.29	0.32	0.30	0.01
Corless B	10	0.24	0.27	0.26	0.01
Tsay Keh	31	0.21	0.36	0.40	0.06
Lafferty	29	0.20	0.43	0.33	0.07
Von Somer	14	0.17	0.39	0.30	0.09
Ospika	5	0.36	0.41	0.39	0.02

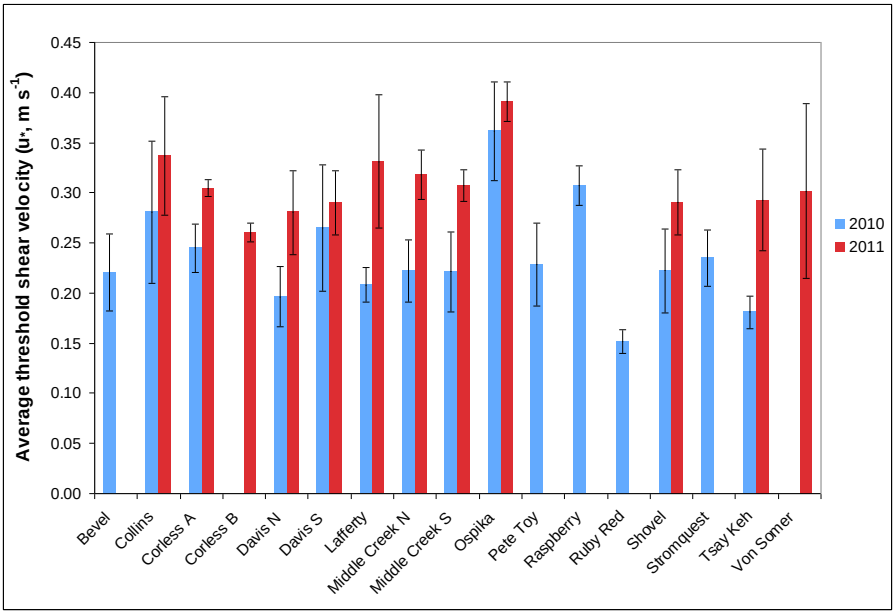

Figure 2.1. The mean threshold shear velocity (u*t, m s-1) for dust for each test site for all valid tests in 2010 and 2011. Error bars represent the standard deviation of the mean.

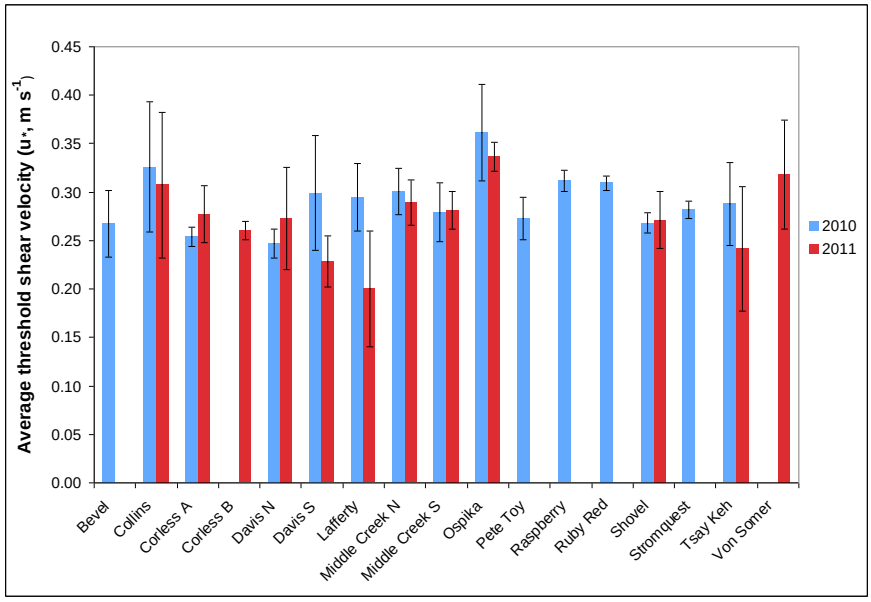

Figure 2.2. The mean threshold shear velocity (u*t, m s-1) for sand for each test site for all valid tests in 2010 and 2011. Error bars represent the standard deviation of the mean.

2.4.3 Emissions of PM_{10} Mineral Dust from the Test Beach Areas

The dust flux, which is the amount of PM_{10} produced per unit area per second from a PI-SWERL test is determined from the measurement of the PM_{10} concentrations (C, µg m^{-3}) and the air flow (V, m^3 s^{-1}) through the instrument, and the known dimensions of the PI-SWERL annular blade (m^2). An emission flux (F, µg m^{-2} s^{-1}) can be calculated as:

$$F_{i,cum} = \frac{\sum_{begin,i}^{end,i} C \times V}{A_{eff}(t_{end,i} - t_{begin,i})} \qquad (2.1)$$

where the summation occurs over every 1 s measurement during level i, beginning at $t_{begin,i}$ and ending at $t_{end,i,}$ with t as integer seconds. The measured dust concentration and flow rate are converted to an emission flux by the effective area of the PI-SWERL, A_{eff}, which is 0.026 m^2. The PI-SWERL tests measure the potential PM_{10} dust emissions from the surface at different equivalent wind shear velocities (i.e., u_*, m s^{-1}). The tests are conducted at pre-set equivalent shear velocities that can span the range 0.1 to 1.2 m s^{-1}. The corresponding wind speed for a u_* of 1.2 m s^{-1} is approximately 90 km hr^{-1} at 2 m above the ground, which would be an extreme wind event. The range used for testing at the reservoir beaches is u_*=0.15 m s^{-1} to 0.46 m s^{-1}, which was determined based on testing to maximize the range but limit the concentrations of PM_{10} to values that did not over-range the instrumentation.

A comparison of emission relationships estimated for beaches in 2010 and 2011 are shown in Figs. 2.3 – 2.13. As these figures show, for all cases the PM_{10} flux (µg m^{-2} s^{-1}) measured in 2010

for the second and third applied shear stresses (i.e., u_*=0.31 m s^{-1} and u_*=0.46 m s^{-1}) is significantly greater than the mean values measured in 2011. To get a sense of the year to year differences in the emissions each year's data are plotted together in Figs. 2.14 and 2.15 and as a percent difference between the years in Fig. 2.16. For the lowest applied shear stress the picture is less clear with both increases and decreases in mean emission potential (Fig. 2.16). In general, it appears that these beaches are capable of producing more dust in 2010 than they

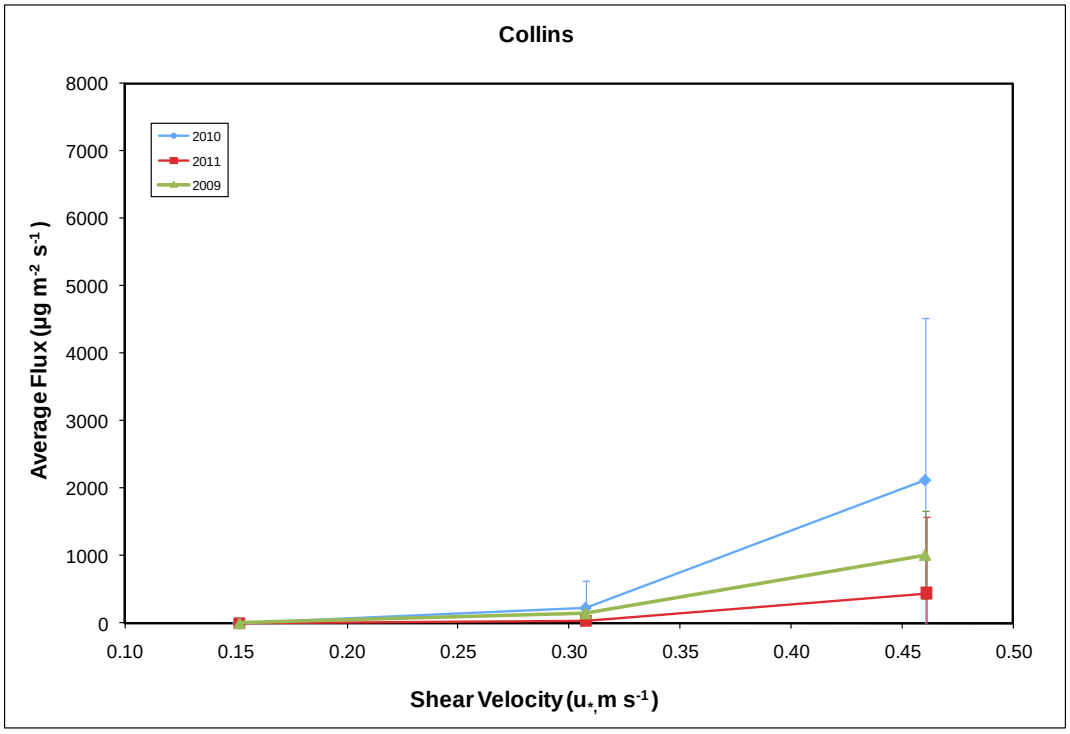

Figure 2.3. The emission relationships Collins Beach for 2009, 2010, and 2011.

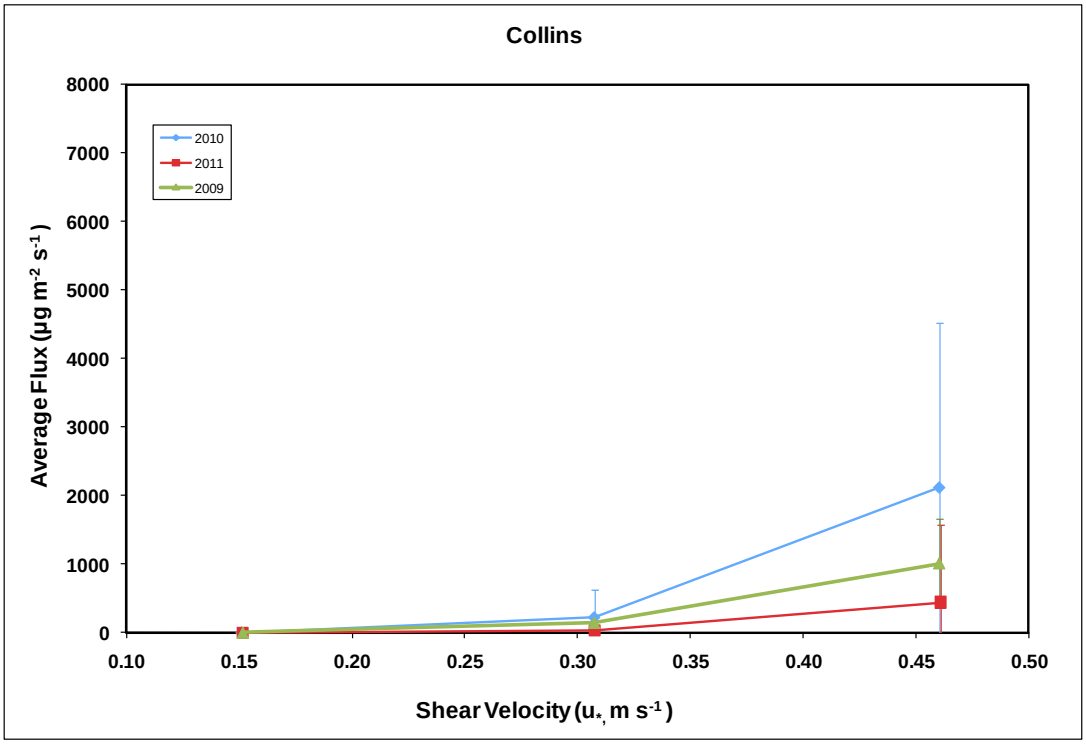

Figure 2.4. The emission relationships Davis North Beach for 2009, 2010, and 2011.

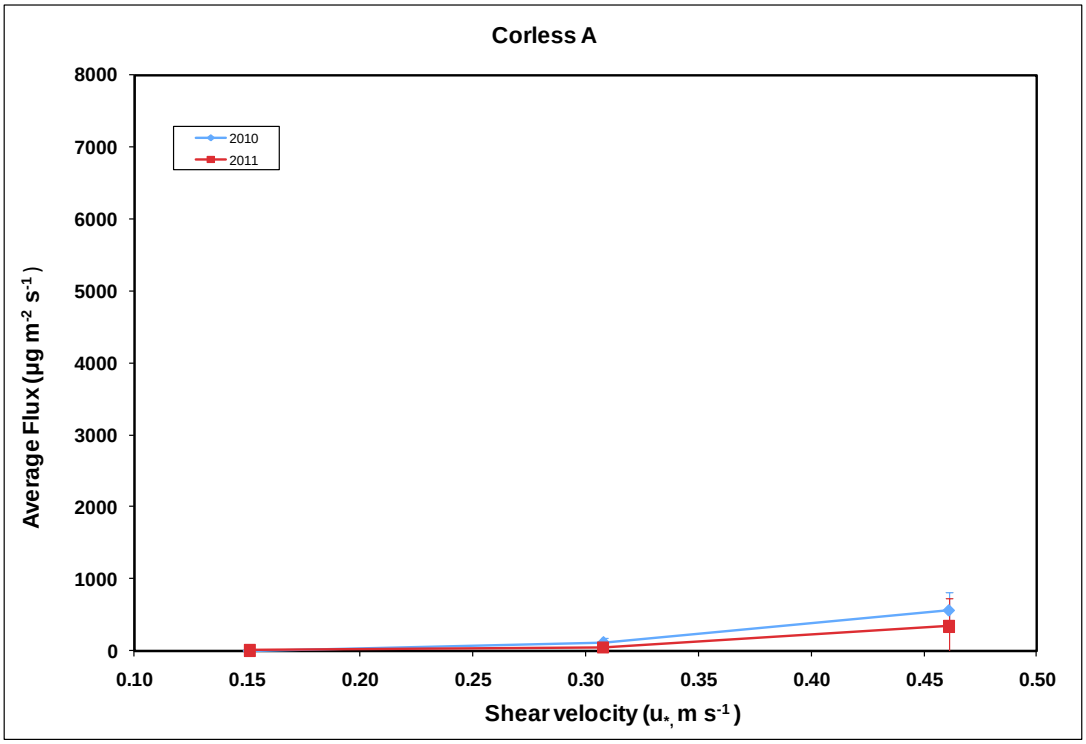

Figure 2.5. The emission relationships Coreless (Lorimer) Beach for 2010 and 2011.

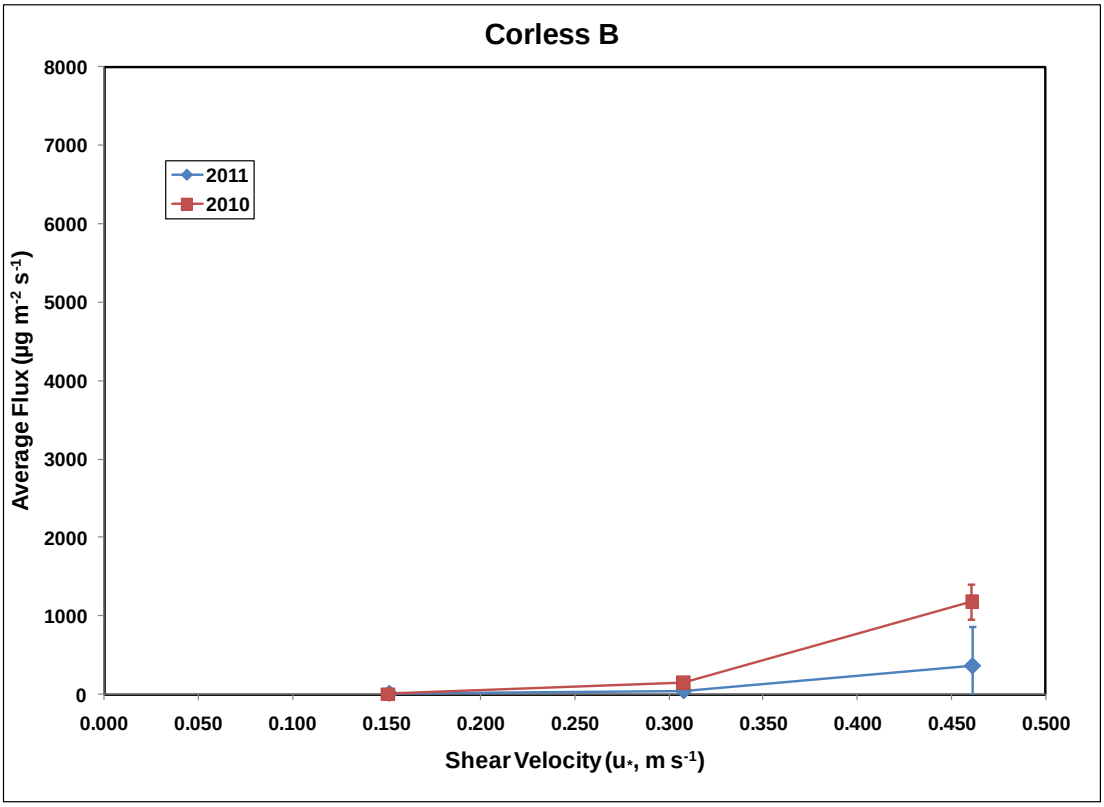

Figure 2.6. The emission relationships Coreless (Stromquest) Beach for 2010 and 2011.

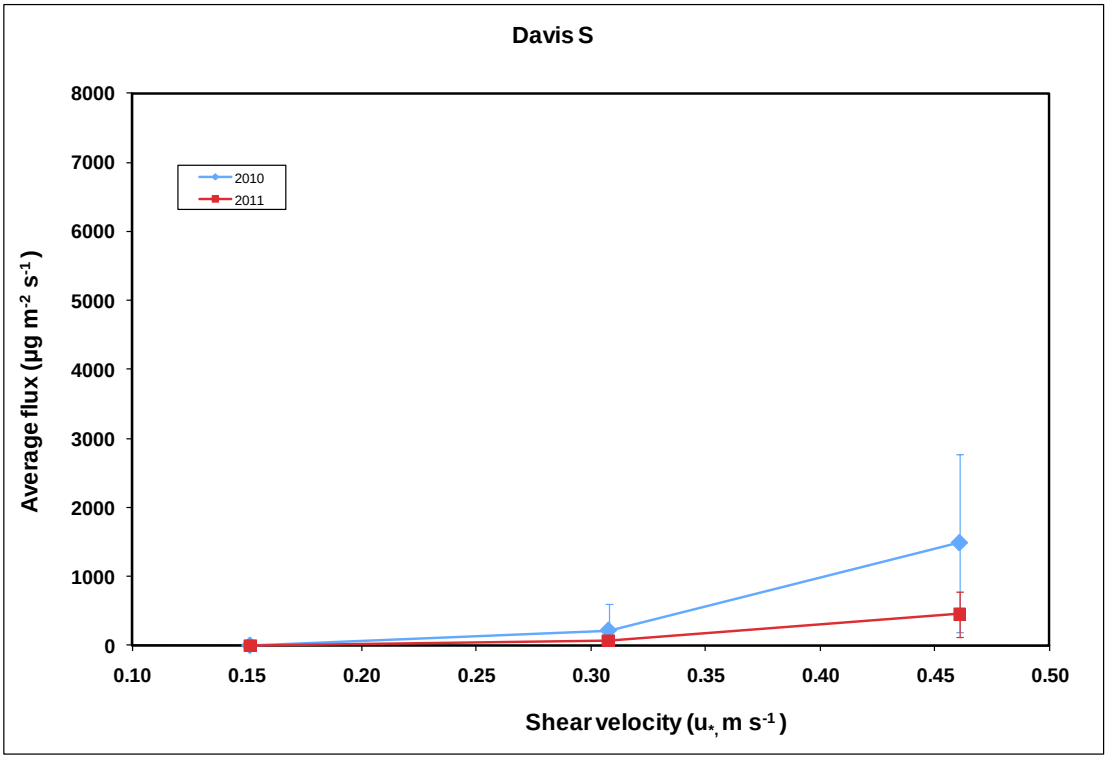

Figure 2.7. The emission relationships Davis South Beach for 2010 and 2011.

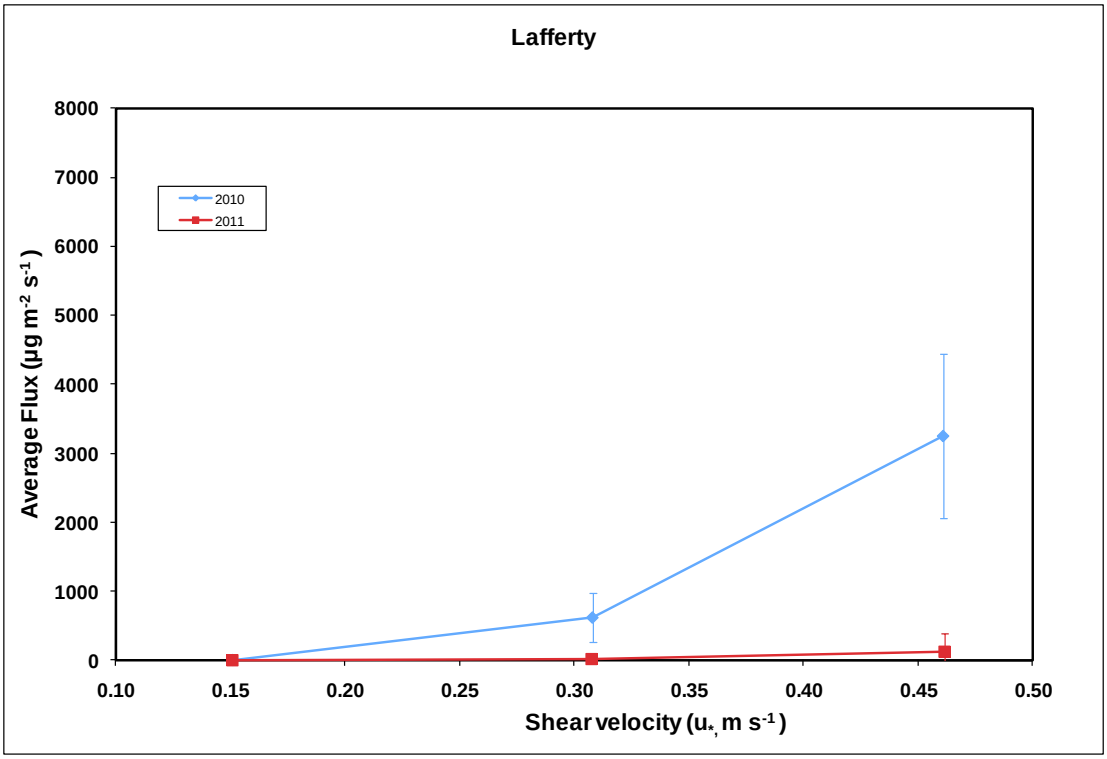

Figure 2.8. The emission relationships Lafferty Beach for 2010 and 2011.

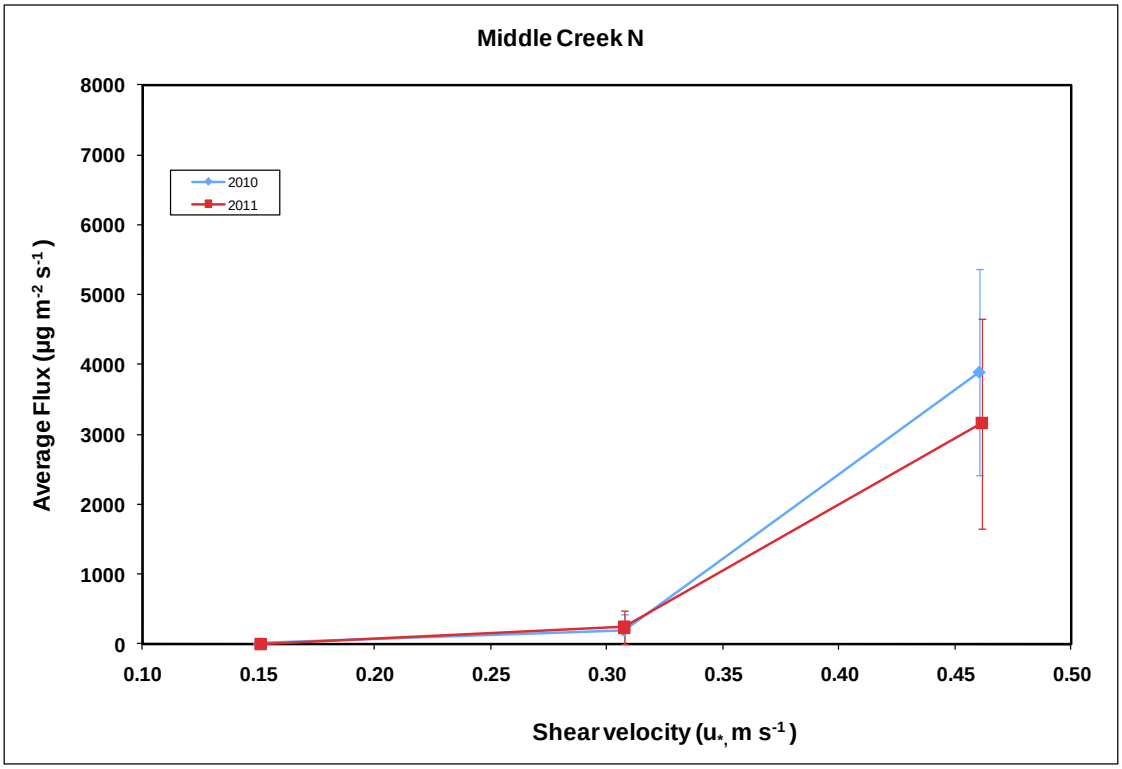

Figure 2.9. The emission relationships Middle Creek North Beach for 2010 and 2011.

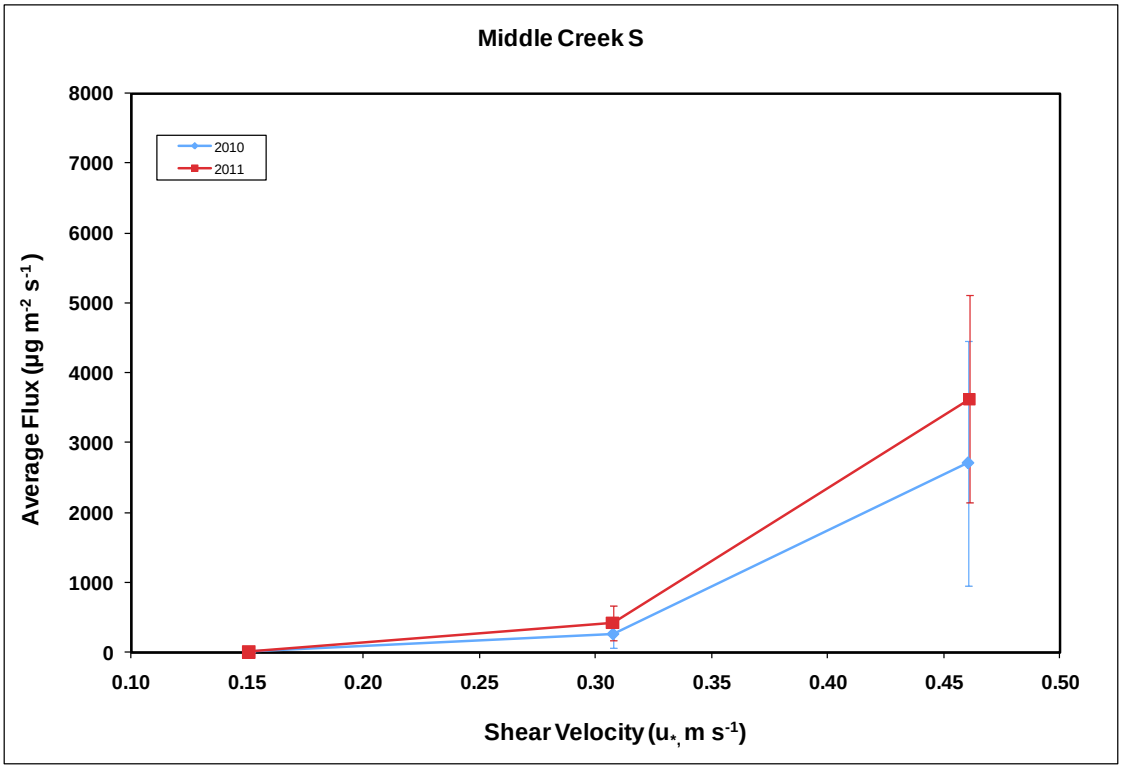

Figure 2.10. The emission relationships Middle Creek South Beach for 2010 and 2011.

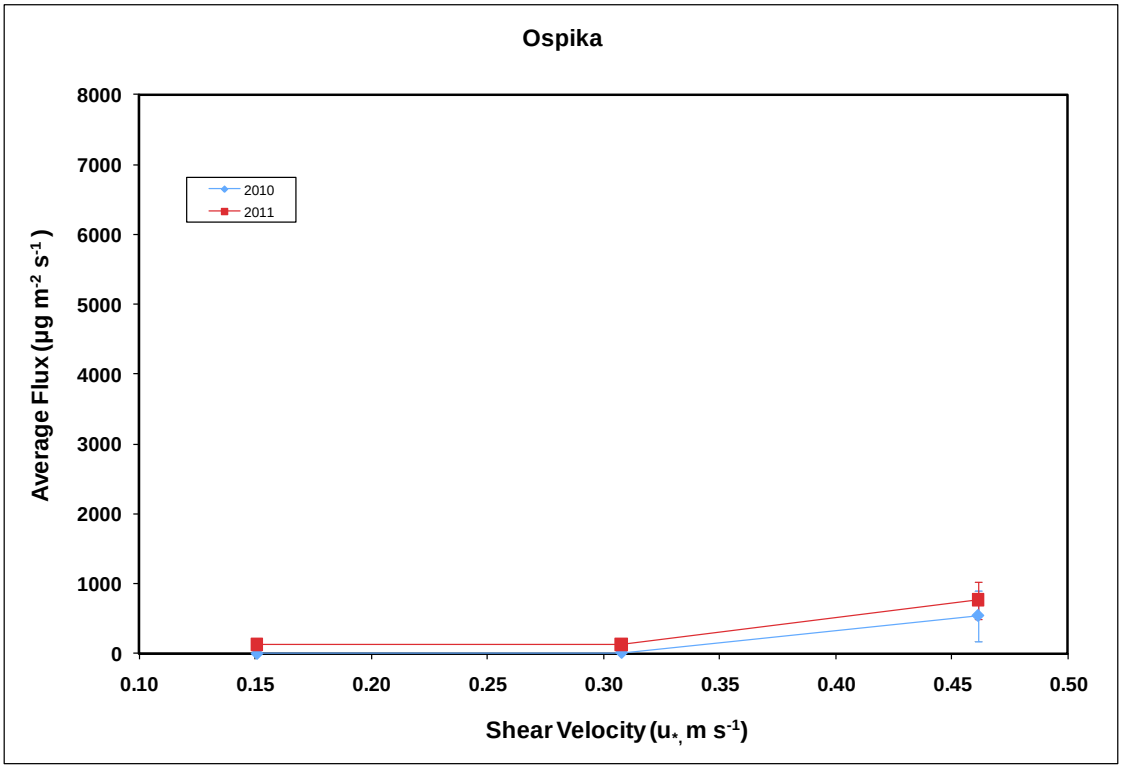

Figure 2.11. The emission relationships Ospika Beach for 2010 and 2011.

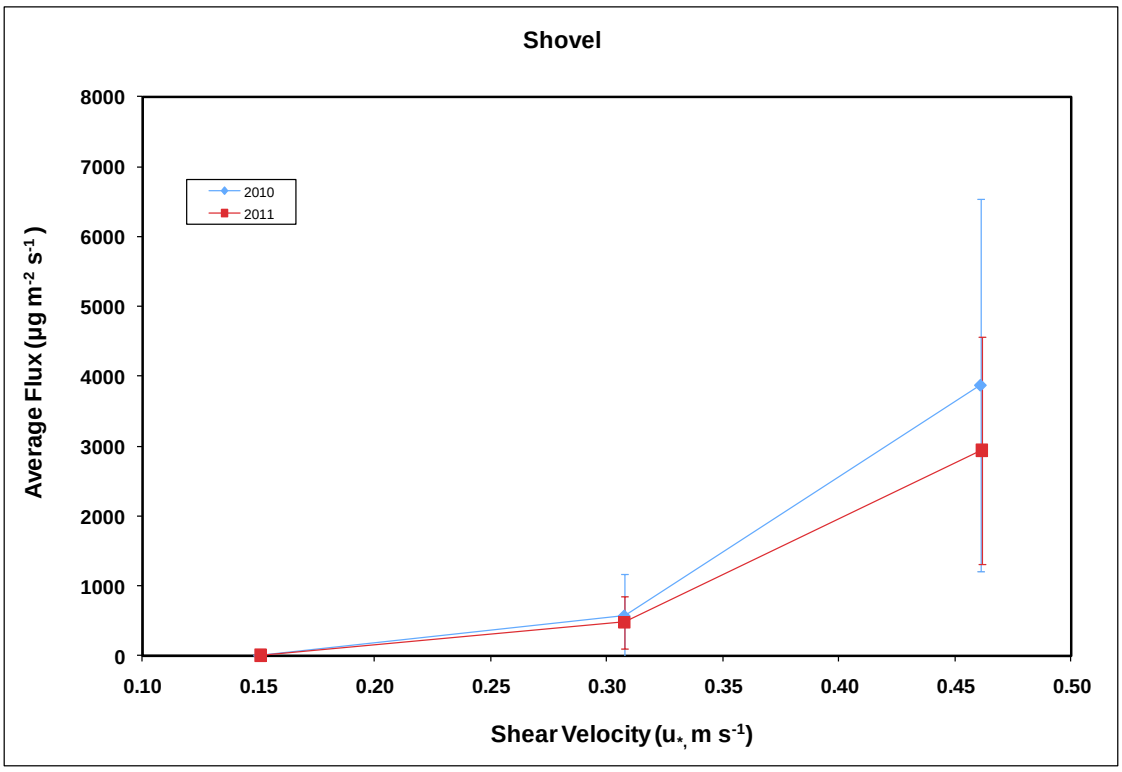

Figure 2.12. The emission relationships Shovel Beach for 2010 and 2011.

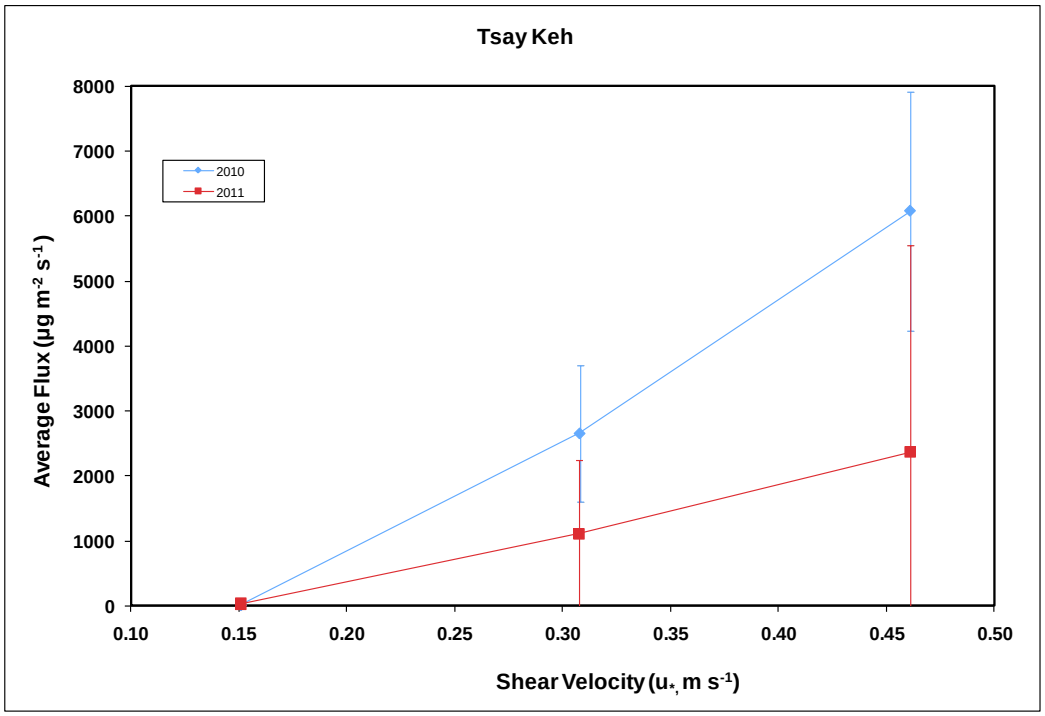

Figure 2.13. The emission relationships Tsay Keh Beach for 2010 and 2011.

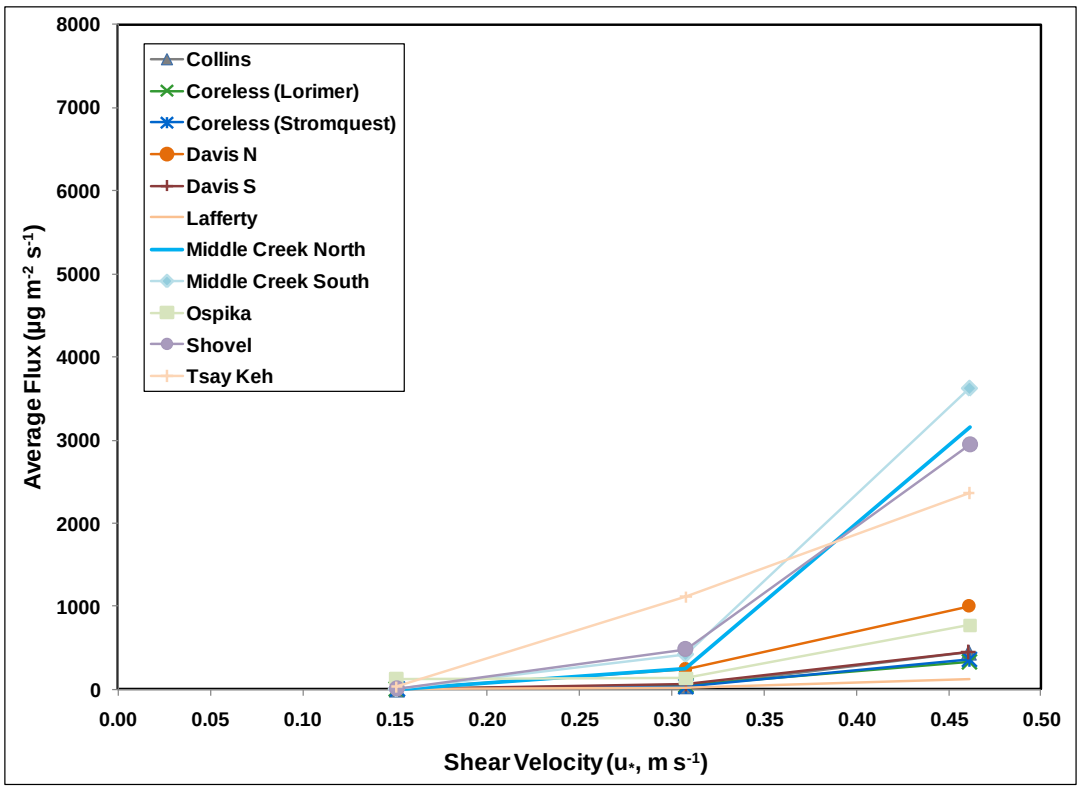

Figure 2.14. The average emission flux as a function of u* for all of the test locations in 2011.

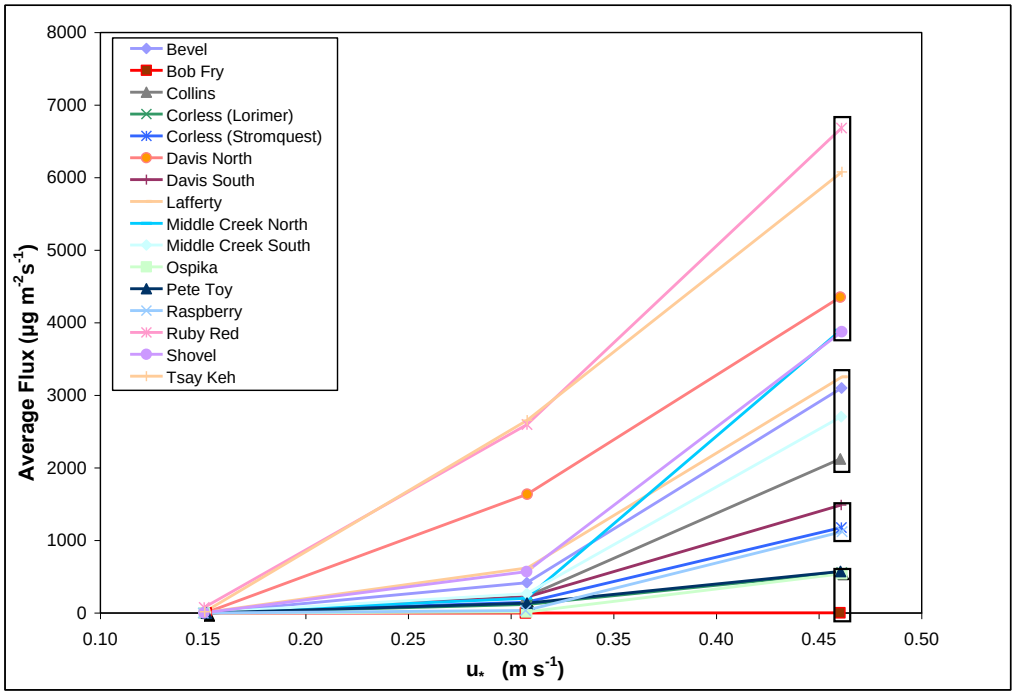

Figure 2.15. The average emission flux as a function of u* for all of the test locations in 2010.

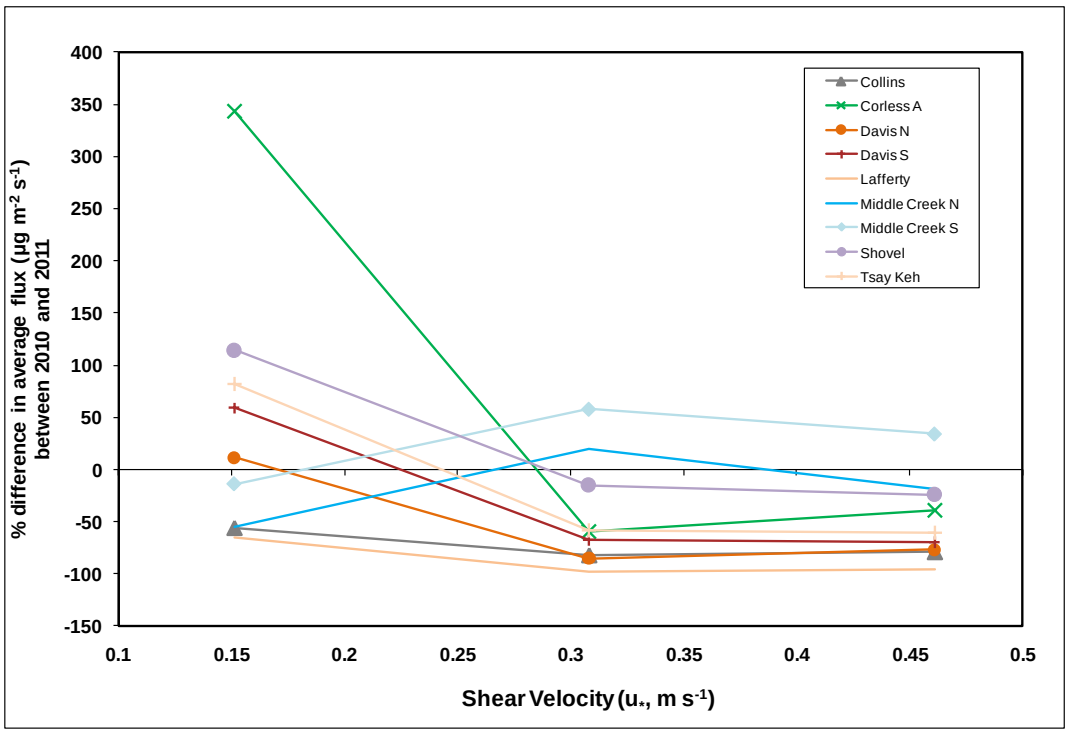

Figure 2.16. The % difference in emissions by location between 2010 and 2011 as a function of shear velocity.

were in 2011. For beaches with comparable data for 2009 (i.e, Collins and Davis N), the emission values measured for the highest shear velocity (0.46 m s^{-1}) are closer to those observed in 2011, but less than those of 2010.

There are several reasons why this may have occurred. The first reason may be that because we did not measure at exactly the same locations from year to year, by chance in 2010, locations that have a higher dust emission potential were tested in 2010 compared with the sites measured in 2011 (or 2009).

A second reason is that the water that inundated the beaches in 2010 had greater amounts of suspended sediment, specifically in the clay fraction, which deposited onto the surface. Small changes in the silt and clay content of the sand of the beaches can translate into large changes in dust emission potential. As described earlier there was a notable decrease in the clay content at each site where data were available for the same beach for both years (Table 2.3). This is consistent with the observation that in general the PM_{10} emission potential was reduced in 2011 compared with 2010. The clay component represents the important reservoir for the dust that can be emitted from the surface under the action of wind and saltating sand.

In most cases the beach surfaces dry out very rapidly at the Williston Reservoir test sites due to the sandy nature of the sediments and wind conditions that promote evaporation. High

moisture content in the surface sediments was only observed when test areas were close to the waterline of the rising reservoir or immediately after precipitation events. In 2010 and 2011 the PI-SWERL testing covered a very similar range of soil moisture contents (Fig 2.17). The majority of the tests (≈80%) in both years were carried out with soil moisture less than 1%, which makes comparing emissions between tests quite reasonable and moisture effects on threshold and emission strength will be low. Interestingly, the moisture contents are similar between years, but the thresholds and emissions are lower in 2011 versus 2010, suggesting that RH could have played a key role in increasing threshold in the cool moist summer of 2011.

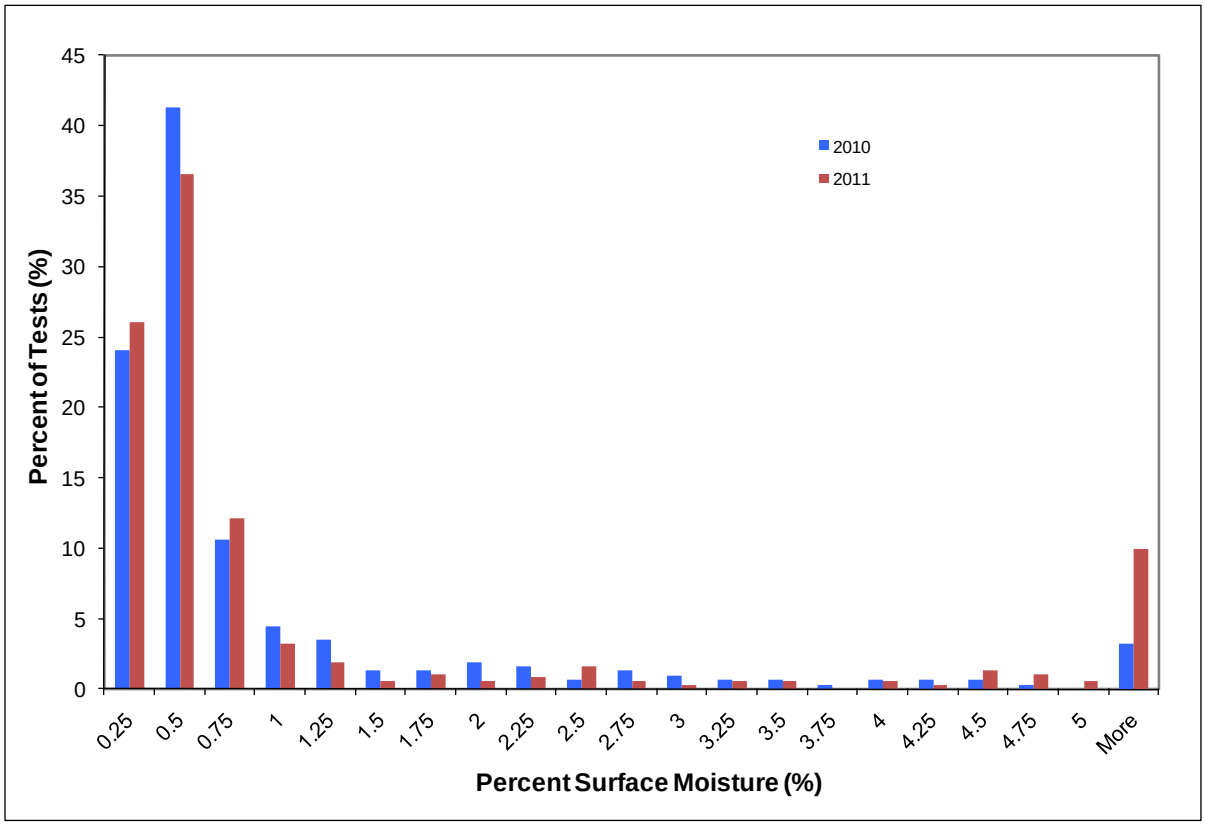

Figure 2.17. Distribution of surface moisture contents for PI-SWERL tests at the Williston Beach test sites in 2010 and 2011.

3.0 DUST EMISSION MODELLING

Quantification of wind erosion and subsequent dust emission is a challenge, particularly in remote regions or over large spatial areas. To better understand wind erosion patterns over large areas, wind erosion models have been developed. This section presents the application of the wind erosion dust emission model (WE_DUST_EM) for the Williston Reservoir Beaches 2011 dust season. This is a mesoscale model that was developed to distribute wind erosion and dust emission data measured during field season research over the entire study domain. Dust emission potential ($\mu g\ m^{-2}\ s^{-1}$) measurements at the Williston Reservoir were completed using the PI-SWERL (Etyemezian et al., 2009). The dust emission relationships measured by the PI-SWERL serve as input to WE_DUST_EM, which outputs data that can be mapped to show the spatial pattern of dust emission 'hot spots' to identify areas with high dust emission potential on Williston Reservoir Beaches (Appendix 1). This is the third year that this model has been used (Nickling et al. 2009 and 2010) and each season the study area has been expanded as the PI-SWERL field tests have extended the number of beaches tested. For the 2011 season, the study area has been extended to include more areas at the northern end of the reservoir (Fig. 3.1), which have greater potential to impact air quality at Tsay Keh than beaches in the southern half of the reservoir. A brief explanation of the WE_DUST_EM model and how it works is provided in Section 3.1 with a more detailed description in Appendix 2.

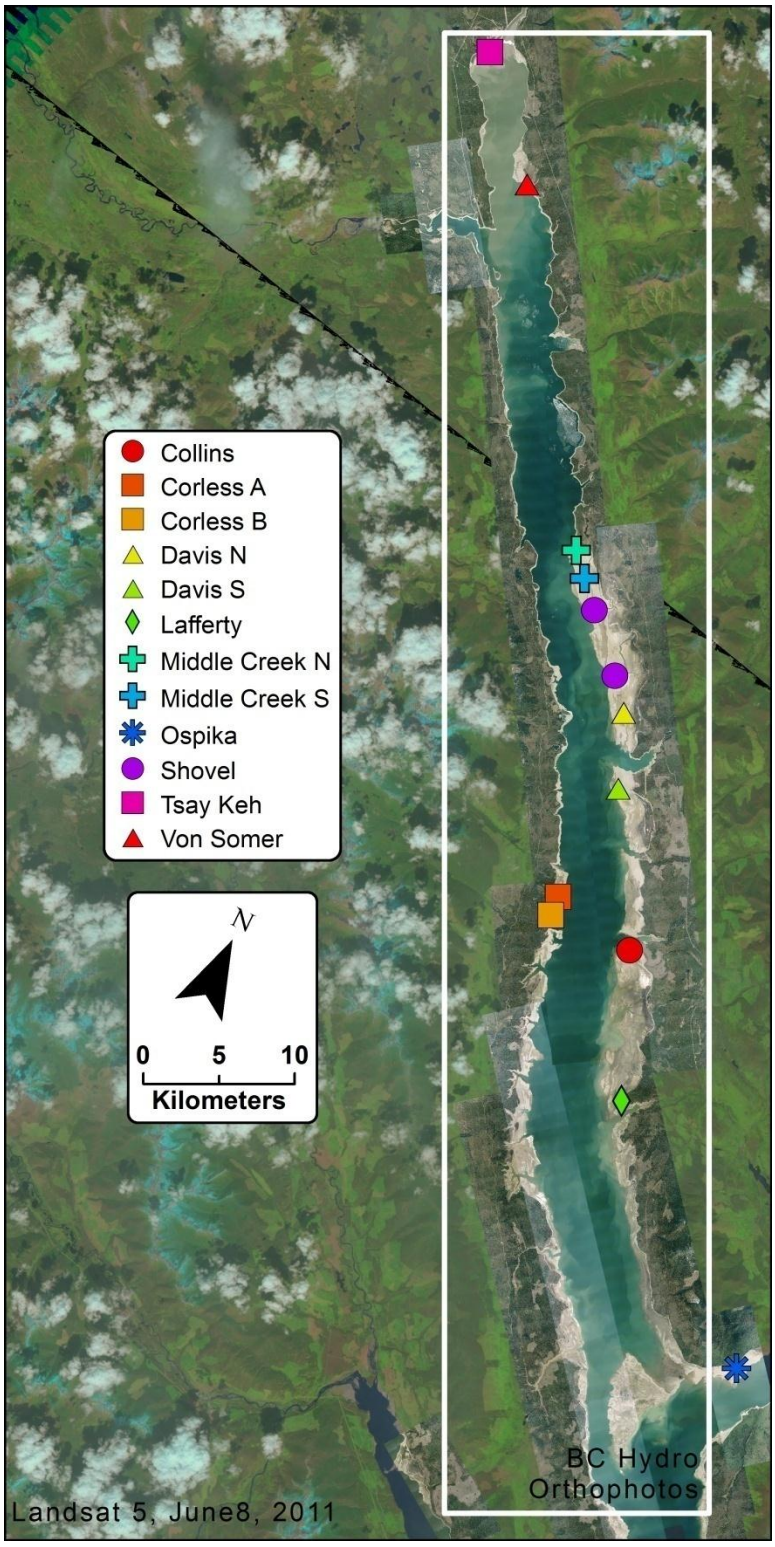

Figure 3.1. Study area and PI-SWERL test sites shown with two Landsat satellite images as the background with an overlay of orthophotos. Data projected to Canada Lambert Conformal Conic coordinate system with WGS84 datum.

Wind erosion and dust emission models simulate the relationship between the erosive forces of the wind and the erodibility of the surface. The WE_DUST_EM model incorporates the heterogeneity of the surface's erodibility characteristics with the wind's erosivity to estimate dust emission potential for the modeled surface. The input data for WE_DUST_EM includes stand-alone models including the California Meteorological Model (CALMET) that calculates wind speed at 10 m above the ground surface, along with field study measurements that are mapped in a Geographic Information System (GIS), and remotely sensed data e.g., aerial photographs. The modelled output of dust emission flux values can then be mapped in a GIS to visually represent the patterns and locations most prone to wind erosion and dust emission.

For this study, the focus is on mapping the dust emission potential of the Williston Reservoir beaches based on the data collected during the most recent field season using the PI-SWERL (Fig. 3.2 a, b, c). The 2011 study area outlined in Fig.3.1 was subdivided into 60 m model grid cells to be consistent with the previous two year's methodology (Nickling et al., 2009; 2010). This resulted in 476,544 grid cells being used to spatially distribute both the model's input parameters and the calculated dust emission output for the beach's 44,069 grid cells. Dust emission potential was modelled for the period of May 20-June 20, 2011 to correspond with the 2011 study period of the PI-SWERL tests and dates where meteorological data were collected at sites on the beaches.

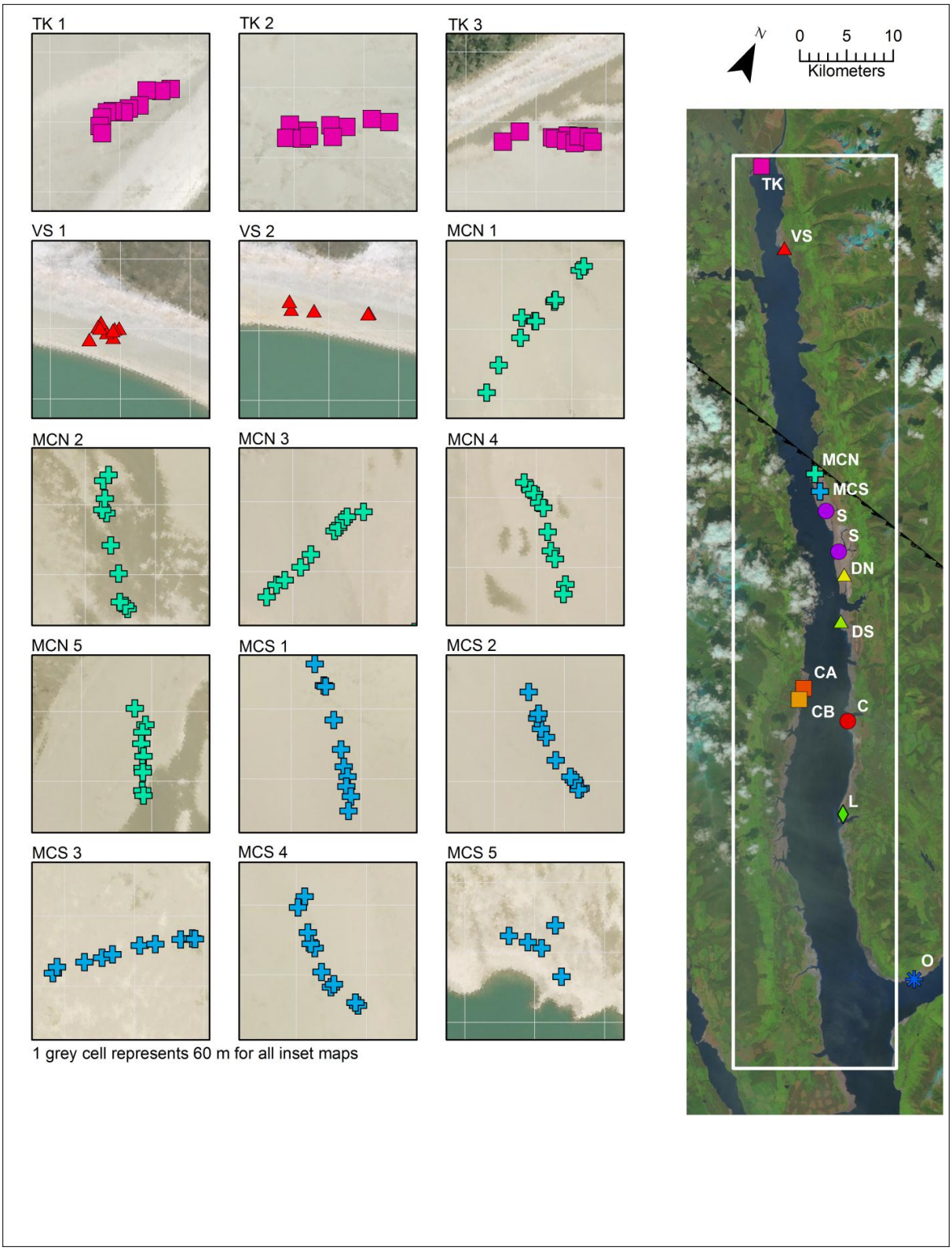

Figure 1.2a. The 2011 PI-SWERL test sites and transects in the upper most section of the study area.

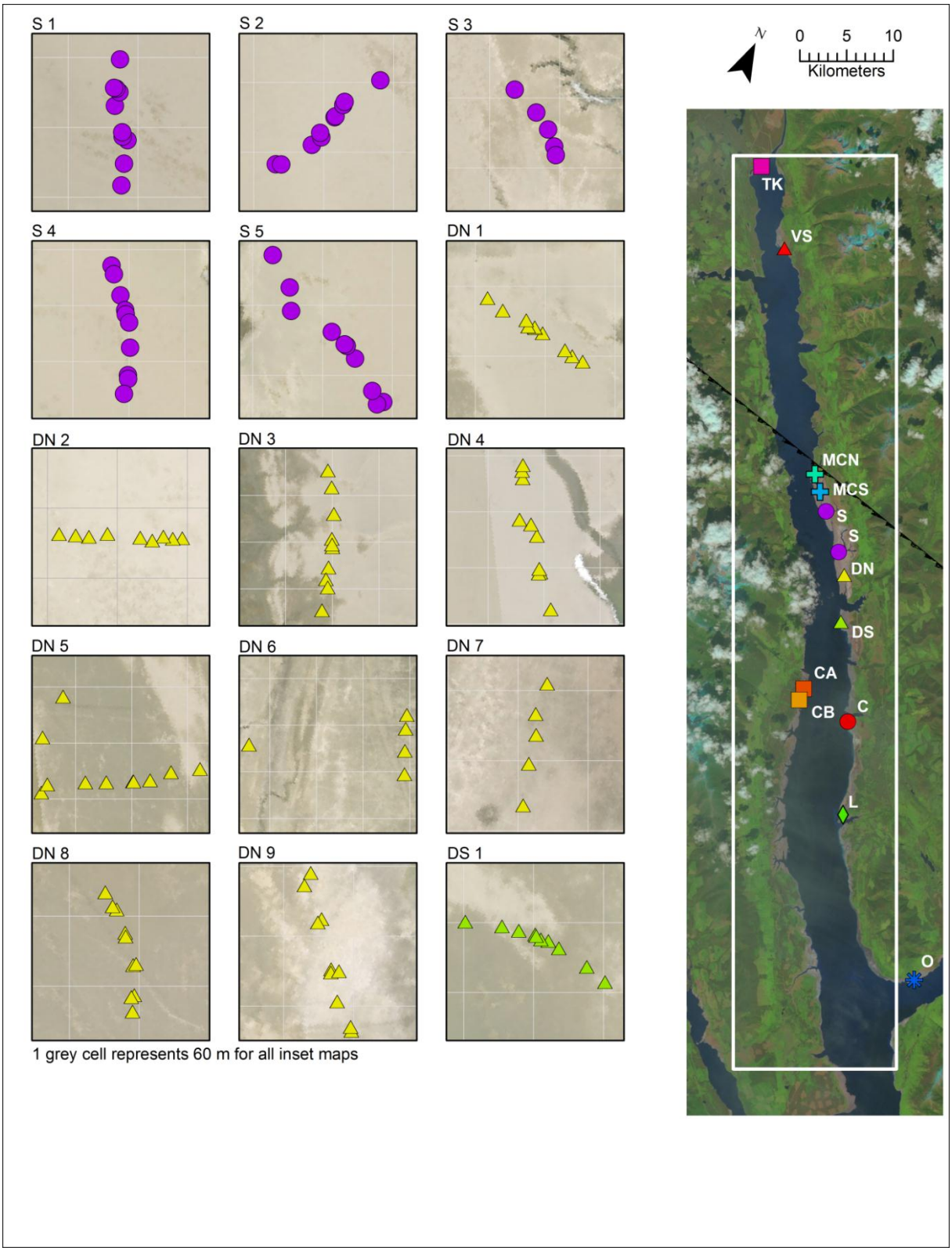

Figure 3.2b. The 2011 PI-SWERL test sites and transects in the middle section of the study area.

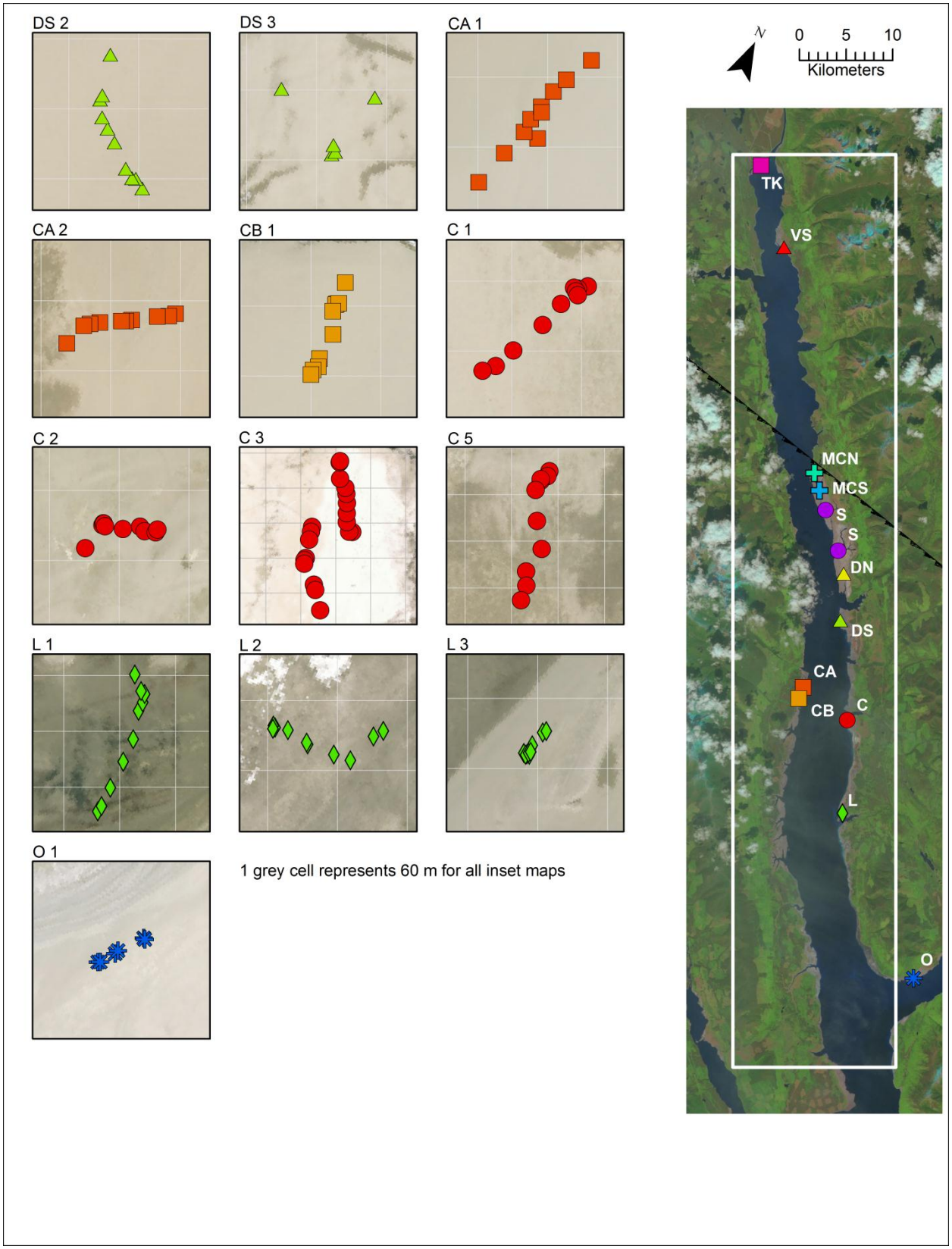

Figure 3.2c. The 2011 PI-SWERL test sites and transects in the lower section of the study area.

3.1 WE_DUST_EM

Wind erosion and dust emission occur when the force of the wind at the surface is sufficient to overcome the resistance of the surface soil particles to movement. An important variable in wind erosion and dust emission research is shear velocity (u_*), which is an indirect measure of the horizontal shearing force of the wind at the surface and is directly related to the change in wind speed (u) with height (z) above the surface (eq 3.2). The shear velocity at which sediment entrainment occurs is called the threshold shear velocity (u_{*t}).

The shearing force at the surface (τ_0) is related to the shear velocity (u_*) by

$$u_* = \sqrt{\frac{\tau_o}{\rho_a}} \qquad 3.1$$

where: ρ_a is air density. An increase in wind speed results in an increase in u_*, which translates into an increase in the shearing force at the surface. Once the shear stress at the surface is strong enough sediment begins to move and the threshold shear velocity (u_{*t}) has been reached. Threshold shear velocity is an important parameter incorporated into many sediment transport equations since it defines the moment soil erosion is initiated. This parameter is a function of the wind's force at the surface and all factors affecting the surface's erodibility. Soil properties that influence the surface's erodibilty include soil texture (i.e., percent sand, silt and clay) and the cohesive aspects of soil moisture or surface crusts. Due to both the spatial and temporal heterogeneity of the surface u_{*t} is not a static value and is best represented by a range of values. Representative ranges of values for a surface soil texture are used in the WE_DUST_EM model and stochastic methods to capture the inherent variability of threshold shear velocities. The shear velocity at the surface can be calculated using the “law of the wall” (von Kármán 1954)

$$\frac{u_z}{u_*} = \frac{1}{\kappa} ln\left(\frac{z}{z_0}\right) \qquad 3.2$$

where: u_z (m s^{-1}) is the wind speed at height z (m), κ is constant (0.4), z_0 (m) is the aerodynamic roughness length, and u_* (m s^{-1}) is the shear velocity. Once threshold shear velocity has been exceeded, the relationship between dust emission (or vertical dust flux, F) and surface shear velocity (u_*) is best described by a power function where F is proportional to u_*. Therefore, dust flux can be calculated by:

$$F = Cu_*^{xsoil} \qquad 3.3$$

where: F is dust flux (μg m^{-2} s^{-1}), C is the constant related to a given soil texture class, and the exponent xsoil is a related to a specific soil texture class.

WE_DUST_EM is programmed in FORTRAN 90 and utilizes equations 3.2 and 3.3 to estimate dust emissions. Five basic input data types are required for the running the: 1) 10 m wind speeds, 2) surface soil texture, 3)aerodynamic roughness length (i.e., z_0 in Eq.3.2), 4) threshold shear velocity (u_{*t}), and 5) dust flux (F calculated by Eq. 3.3). The sources for these data are summarized in Table 3.1 and a description of each component is provided Section 3.2. The model's flow structure or order of operations is described here and depicted in Fig. 3.3. The model is programmed to run at an hourly time step for 24-hour periods. For each hourly time step, the 10 m wind speed data are read into the WE_DUST_EM program. The shear velocity for each model grid cell is calculated using equation 3.2. The minimum threshold shear velocity (u_{*tmin}) measured during the field season is then used to control whether or not to run further calculations. If all the calculated u_* values fall below u_{*tmin} there is no entrainment because none occurred below this u_* value for any location within the study area during the field season. Therefore, if all the u_* values for a given hour fall below the u_{*tmin}, then there is no wind erosion for that time step and the model moves on to the next time step. If any shear velocity value is above u_{*tmin}, the program continues by generating a range of threshold shear velocities for each soil texture class based on a Gaussian distribution. The parameters defining these distributions are based on the PI-SWERL field study measurements (Tables 2.3 and 2.5 3).

These u_{*t} values are used to assign each model grid cell a u_{*tsoil} value drawn randomly from the Gaussian distribution for that soil texture class. If the u_* value for a model grid cell exceeds u_{*tsoil} assigned to that cell then the model determines that erosion can take place. Dust flux is calculated using the power relationship between u_* and F described by equation 3.3 for each model grid cell. For those cells in which the calculated u_* value exceeds the u_{*t} the result is written to the output file. For those cells where u_* does not exceed u_{*t} there is no erosion and a value of zero is entered in the output file. The program moves on to the next hourly time step and continues executing until the end of the 24 period.

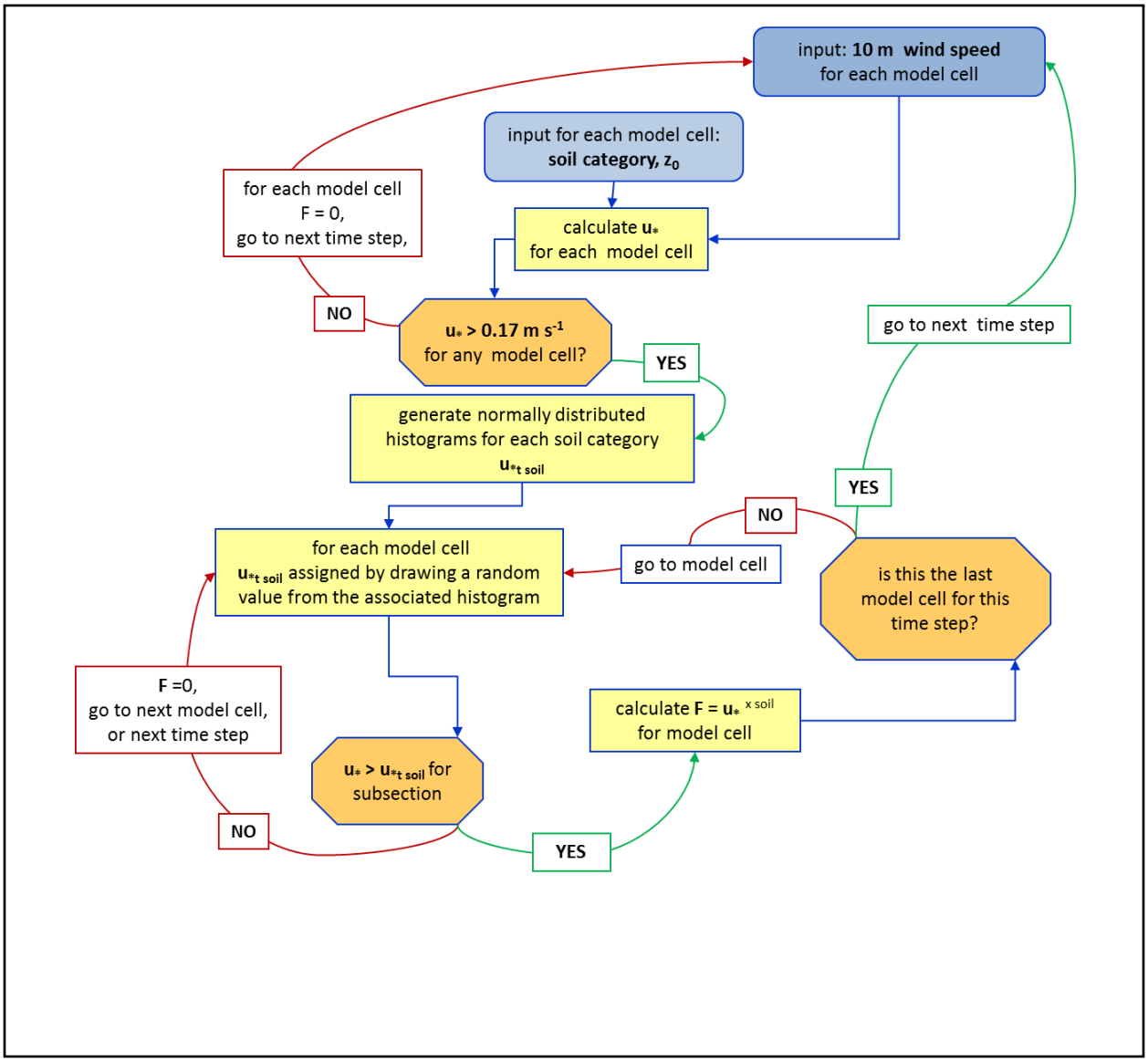

Figure 3.3. Computational flow of WE_DUST_EM model.

1.2 Model Input Parameters

As noted above, WE_DUST_EM requires four basic input data types: 1) 10 m wind speeds, 2) land cover attributes (soil texture and aerodynamic roughness length), 3) u_{*t} and 4) F data. The sources for these data are summarized in Table 3.1 and descriptions of each component are provided in this section.

Table 3.1. Summary of WE_DUST_EM model input parameters and their sources.

Data Type	Model Parameter	Description	Source
Wind	10 m wind speeds	CALMET gridded 10 m wind speed output; (wind.dat)	Generated using CALMET
	Shear velocity (u_*)	Derived from 10 m wind speeds using (Eq. 1.2); Calculated in WE_DUST_EM	CALMET Gridded 10 m wind speed output
Land cover	Surface soil texture	Generated using GIS; input for DUST_EM (surface_att.dat)	Soil texture analysis of samples collected at PI-SWERL tests 2011
	Surface roughness length (z_0)	Derived from meteorological tower data (2010); input for WE_DUST_EM	Williston meteorological data collected as part of the Tillage Study (2010)
Threshold shear velocity	Threshold shear velocity of soil (u_{*tsoil})	Minimum, mean and standard deviation each surface soil texture class; input for WE_ DUST_EM	PI-SWERL tests 2011
	Minimum threshold shear velocity (u_{*tmin})	Minimum threshold shear velocity for study site; input for WE_ DUST_EM	PI-SWERL tests 2011
Dust Flux	Constants and exponents in power function	Power function where F is proportional to u_* for each soil texture class (eq. 1.3); input for WE_ DUST_EM	PI-SWERL tests 2011

3.2.1 Study Area Wind Speeds-CALMET

WE_DUST_EM does not have its own meteorological model and therefore a standalone model is used to generate 10 m wind speeds for each grid cell modelled. The model used is the most recent version of the EPA-approved CALMET (version 7.12.0.03_08_2011) as has been done for the past two seasons (Nickling et al. 2010 and 2011). CALMET is the meteorological component of the CALPUFF air dispersion modelling system (url: http://www.src.com/calpuff/calpuff1.htm, accessed Jan. 17/12). CALMET offers several pre-processing algorithms to convert common data formats for meteorological, land use and elevation data sets used in the United States into input files for the CALMET model. However, there are no pre-processors that read the data formats available in Canada, and some of these pre-processors do not accept user-defined data sets. Therefore, for applications outside of the United States most of input data must be manually reformatted and sometimes manually constructed before it can be used in CALMET. For example, all the surface station data must be manually reformatted into files required by the pre-processor SMERGE to generate the surface.dat input file for CALMET. The geophysical data that describes the terrain and land use/land cover of the study area has four pre-processors however none of these are designed for use with user-defined data sets or data set outside of those in use in the United States. Therefore, the geo.dat input file for CALMET must be manually generated. The manual generation of these files is a time consuming task. Once all the input files for CALMET have been generated the model is used to generate hourly wind field grids with algorithms that utilize surface and upper air meteorological data including wind speed and direction, air temperature and pressure, relative humidity, cloud ceiling and cover along with surface elevation and land cover data.

Meteorological Input Data:

For the Williston Reservoir one upper air station, Prince George, BC, and five surface meteorological stations were used as input data to CALMET. The meteorological data collected at three on-site surface Partisol instruments (i.e., wind speed, wind direction, temperature, and atmospheric pressure measured at 2 m) along with complimentary data from the Chetwynd and Mackenzie airports, BC, provided the surface station input data required by the CALMET model. CALMET requires 10 m wind speeds, which necessitated that the winds measured on or near Reservoir beaches be converted to 10 m equivalent values. This was accomplished by applying the following equation:

$$U_1 = U_2 \frac{ln\left(H_1/z_0\right)}{ln\left(H_2/z_0\right)} \qquad 3.4$$

where: U_1 is the wind speed to be calculated; U_2 is the measured wind speed; H_1 is the height of the wind speed to be calculated (10 m); H_2 is the height of the measured wind speed; and z_0 is the aerodynamic roughness length.

The Partisols do not collect cloud ceiling height and cloud cover data and at least one surface station is required to have these data for each time step. In the previous years (Nickling et al. 2010 and 2011) the Mackenzie airport data set contained ceiling height and cloud cover data and fulfilled the data requirements of CALMET by supplying these data missing from the local meteorological data. However, in January 2011 Environment Canada began using partnered station data for the Mackenzie Airport site and this data set no longer includes ceiling height and cloud cover. Climate Services at Environment Canada suggested a substitute airport, Chetwynd, which includes ceiling height and cloud cover however, these data are only collected for 12 hours a day between 7am and 7pm. Therefore, for the hours where these data were missing the 7pm data were used to fill the gaps.

Table 3.2 CALMET input data

Data Type	Model Parameter	Description	Source
Surface	Digital elevation data	1:50 000 scale, geographic coordinate system, and NAD83 datum; input for CALMET (geo.dat)	GeoBase® (http://geobase.ca)
	Land cover data	Generated visually via digitizing from orthoimagery; input for CALMET (geo.dat)	BC Hydro, 2009
Meteorological	Surface stations	Mackenzie Airport, BC, Chetwynd Airport, BC & three on site Partisols; input for CALMET (surf.dat)	Environment Canada & Williston meteorological data collected as part of the Williston Regional Air Quality Monitoring Program
	Upper air station	Prince George, BC; input for CALMET (up.dat)	http://weather.uwyo.edu/upperair/sounding.html

Surface Cover and Terrain Input Data:

Surface elevation data for the study area (Table 1.1) were acquired from GeoBase.ca at 1:50,000 scale, geographic coordinate system, and NAD83 datum. These data were projected and clipped in ArcGIS to match the study area boundaries, projection, grid cell resolution using the nearest neighbour re-sampling technique (Lillesand and Kiefer 2000).

Vector land cover data were digitized using ArcGIS at 1:25,000 scale from 1:25,000 scale BC Hydro (2009) orthoimagery. Prior to digitizing individual orthoimages were mosaiced together at 2 m grid cell resolution and projected to match the study area. Digitized land cover data were assigned USGS land use/land cover codes (forest- 40, reservoir - 53, beach - 72) and converted to raster format with a grid cell resolution of 240 m. Figure 3.4 shows the land cover and study area extent for both the 2011 and 2010 project years. The beach coverage fluctuates with the rise and fall of the reservoir water therefore the extent of the beach used as input for the model varies depending on the height of the water when the land cover is classified. In 2010, the method for classifying land cover was unsupervised classification of LandSAT Thematic Mapper data acquired May 4th, 2010 (LandSAT 5 Path 50 Row 21) (Nickling et al. 2010). Some of the variation in the extent of the beach cover can be attributed to the different methods used to extract these data and the rest due to the fluctuation in water levels in the spring prior to the beaches reaching high pool.

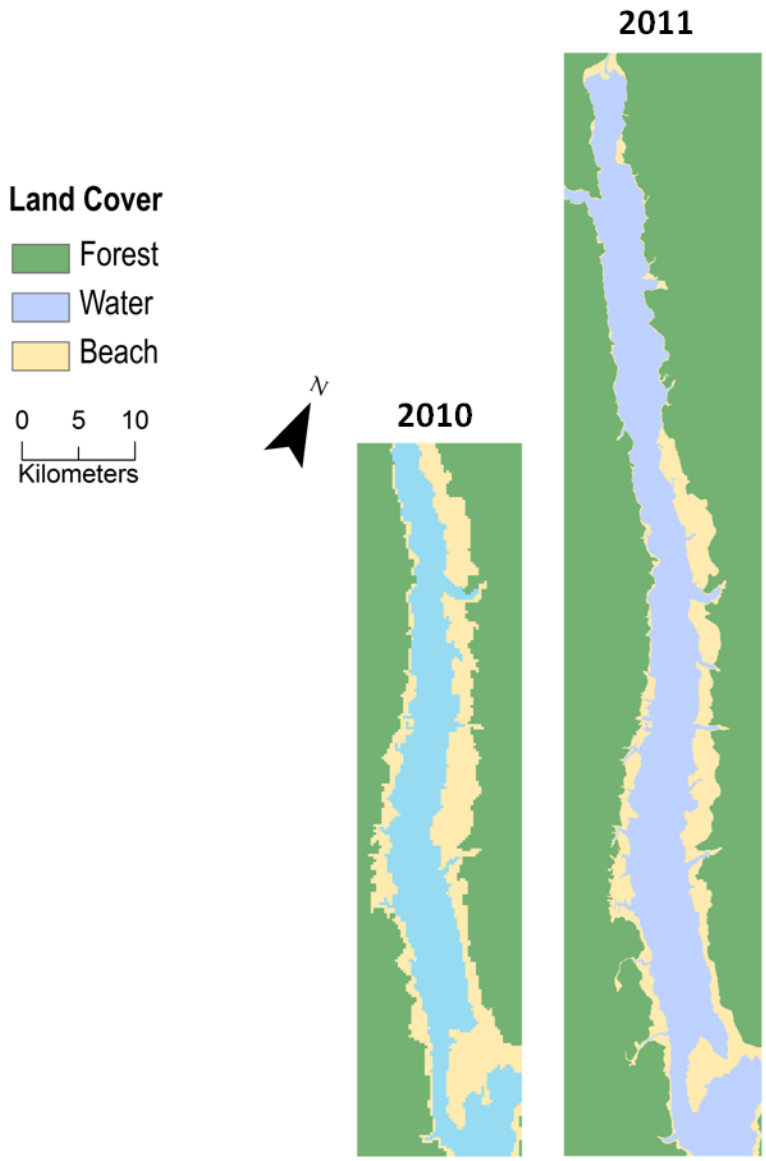

Figure 3.4 Landcover classifications for both 2010 and 2011.

CALMET limits the number of columns and rows that can be modelled to 265 in each direction. With a model grid cell resolution of 60 m there are 1632 rows and 292 columns, far exceeding CALMET's limit. An attempt was made to recompile the FORTRAN code to extend these boundaries but there were too many compiler dependent functions for this to be successful. Therefore, a test run was done with the study area subdivided into a top and bottom section and the model grid cell size increased to 240 m (resulting in two parts with 204 rows and 73 columns each). Once the 10 m wind speed output had been generated, each 240 m grid cell is sub-divided into four 60 m grid cells. To test whether filling in the data gaps for the cloud height and cover input along with the parsing of the larger CALMET model grid cells into the smaller

WE_DUST_EM grid cells would significantly affect the output of the CALMET model an evaluation was carried out using the standard error of the estimate method described below.

Model Evaluation:

To assess how well the modified methodology using CALMET simulated 10 m wind speeds for the study area compared to the measured or observed wind speeds, the standard error of the estimate (SEE) was used. This a method used to quantify the difference between the observed wind speeds (measured at one of the Partisol stations) with the wind speeds generated for that location by CALMET. For this assessment, June 13, 2011, a day where high wind speeds were measured was chosen. For this day the CALMET output for the 60 m grid cell containing one of the Partisol instruments whose meteorological data were not included as input to CALMET, the Davis Beach Partisol site was chosen. This site was chosen because the Davis Beach Partisol meteorological data set did not cover the entire May 20 -June 20 modelling period and therefore was not used as input for CALMET, but did have data for June 13, 2011. The SEE value indicates the overall magnitude of error in the estimated wind speed by squaring the difference between the observed (Wsd_o) and modeled wind speed (Wsd_m):

$$SEE = \sqrt{\frac{\sum_{i=1}^{n} (Wsd_o - Wsd_m)^2}{n}} \qquad 3.5$$

A SEE value of 0.0 would indicate that the observed and modeled wind speeds are in perfect agreement. If these data were plotted on a graph they would line up perfectly on the 1:1 line. In this application, the SEE value was 0.5 showing good agreement between the modelled 60 m grid cell wind speeds and the measured wind speeds at the location of the Davis Partisol station (Fig. 3.5). There is some scatter about the 1:1 line, however the good agreement shown by the SEE test is also reflected in the R^2 value of 0.90. Therefore, the 10 m wind speeds for the WE_DUST_EM wind input data were generated by CALMET at a 240 m resolution and then parsed into 60 m grid cells.

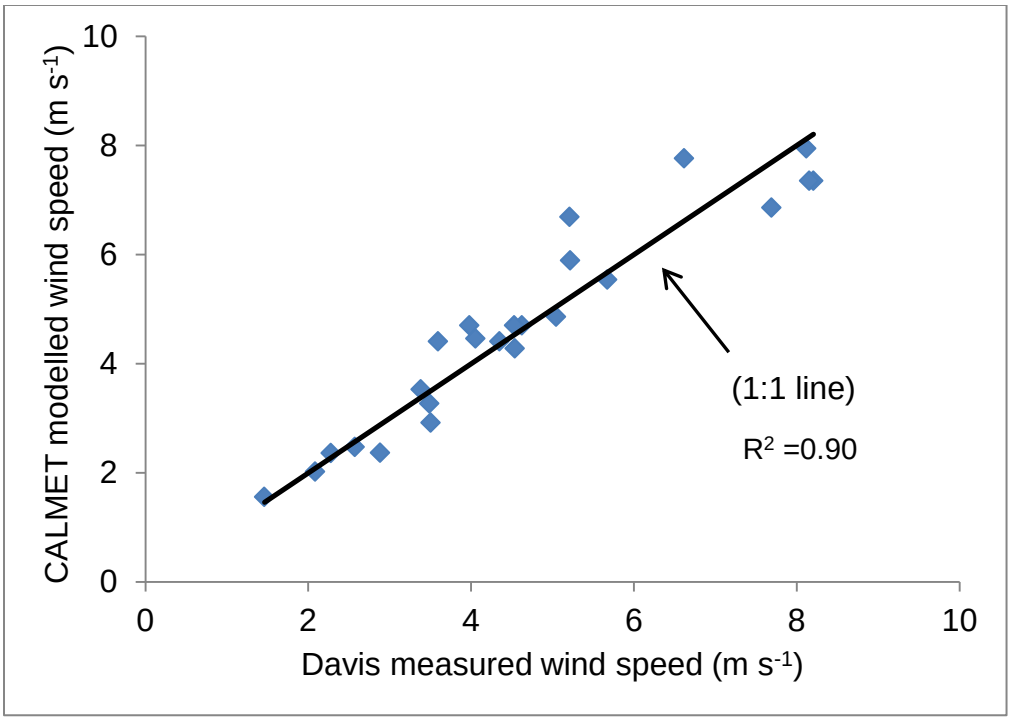

Figure 3.5. Comparison of CALMET generated and observed 10m wind speeds for the Davis Partisol site, June 13, 2011.

Once all the hourly 10 m wind speed data were generated, a post processor provided with the CALMET system can be used to generate output file in a comma-delimited format. These files are then reformatted into input files for the WE_DUST_EM model.

3.2.2 Field Study Measurements

Soil Texture Classes:

To calculate the dust flux potential for the entire study area, surface soil texture classifications are used to link the data measured by the PI_SWERL at test locations with the untested beaches. Surface soil samples from each PI-SWERL test location were analysed and classified based on their content of sand, silt, and clay. Using a GIS method called Euclidean Allocation, which is based solely on the proximity of the 60 m model grid cells to a known soil texture, was used to spatially distribute the data collected at each PI-SWERL site. Soil texture is not used as input for CALMET therefore there was no need to use model grid cells of 240 m and 60 m cells were used directly. Fig. 3.6 shows the classified surface soil texture map generated using this technique for the 2011 season along with the percent cover of each soil class for the beaches and the PI-SWERL sites used for the Euclidean Allocation algorithm. Additional data, including

the threshold shear velocities for entrainment and dust flux values for each soil texture were derived from the PI-SWERL tests carried out in the spring of 2011. This season`s soil sampling yielded four soil texture classes: Sand, Sandy Loam, Loamy Sand and Silty Loam (Table 3.3), one less than the 2010 season where an additional clay texture was identified for a few test sites. (Fig. 3.6). The differences in the soil texture samples collected in 2011 will affect the spatial distribution of surface soil generated by the Euclidean Allocation (Fig. 1.7). For example, Davis North was classified as Sandy Loam in 2010 but Sand in 2011 indicating that the sediments were somewhat lower in silt and this difference means that this section of beach is represented by different soil textures. Fig. 3.7 shows the changes in the soil texture classification maps between 2010 and 2011. These differences will affect the spatial dust emission patterns calculated for beach because the WE_DUST_EM emission parameters are based on soil texture and measured u_{*t} and the relationship between u_* and F as discussed below.

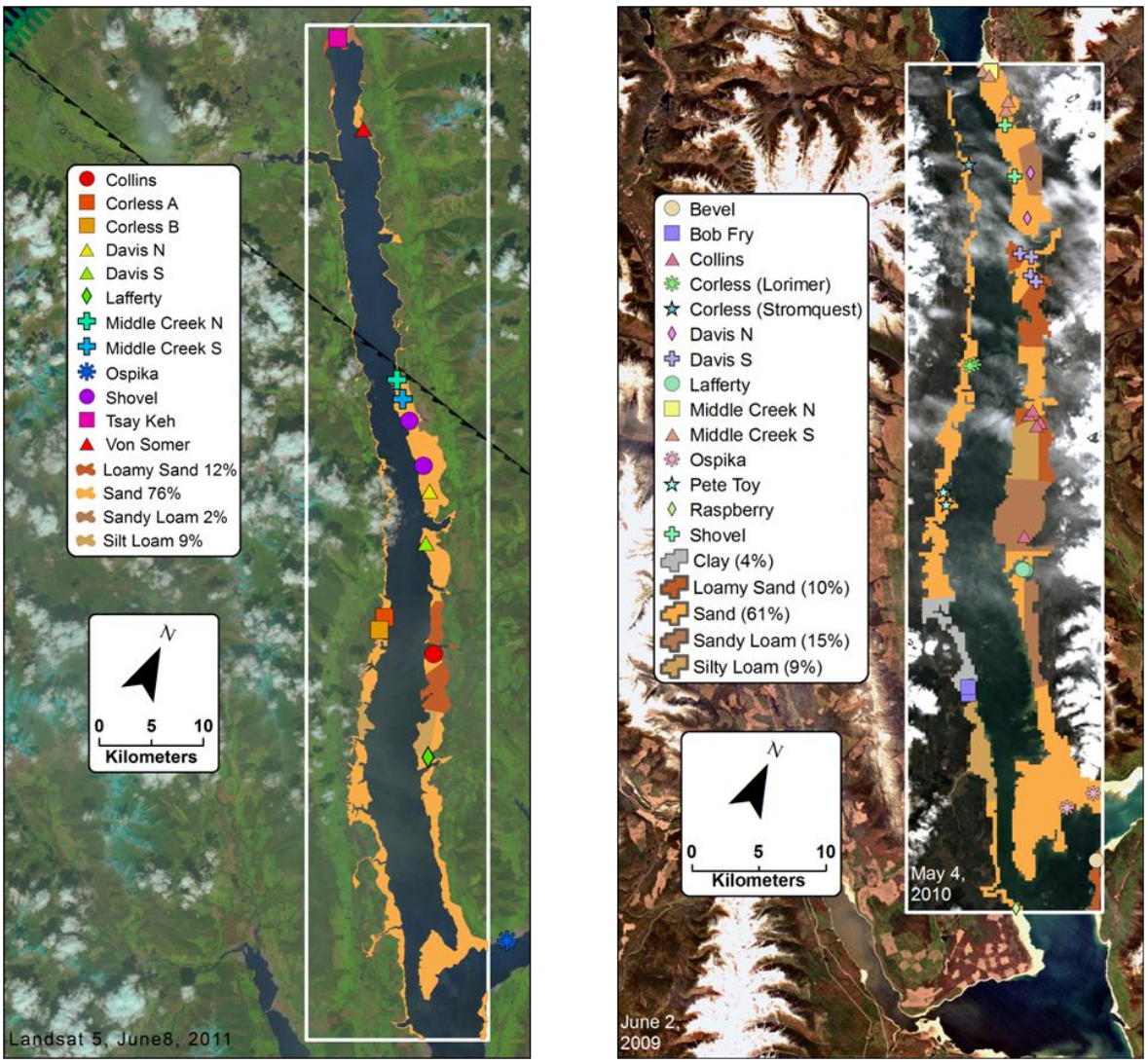

Figure 3.6. Surface soil texture maps with the percent of coverage for each class and associated PI-SWERL test sites 2011 and 2010.

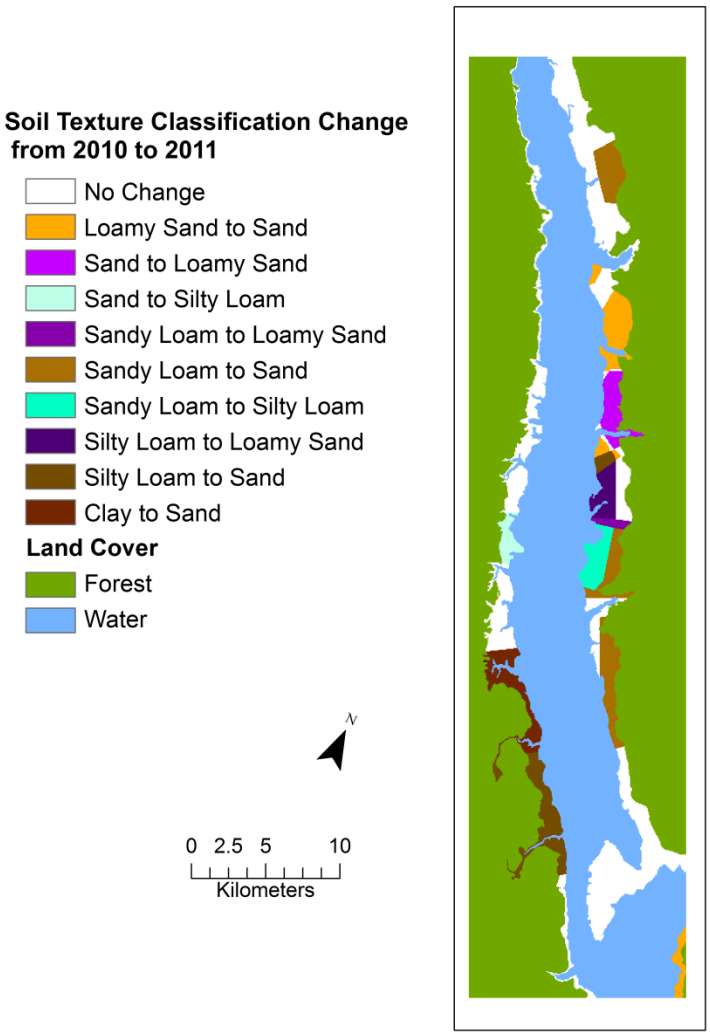

Figure 3.7. Changes in Soil Texture Classification between seasons associated PI-SWERL test sites 2010 and 2011.

Threshold Shear Velocity

Measurements of the threshold friction velocity (u_{*t}) for dust emission measured at each PI-SWERL test site are summarized by surface soil texture in Table 3.3. The ranges of threshold shear velocities associated with the soil texture types measured this season compare favourably with 2010 and are in agreement with measurements from other field studies for soils of similar texture (e.g., Gillette et al. 1980; Gillette and Passi 1988).

Table 3.3. Relationship between surface texture and threshold shear velocity (u*t) measured with the PI-SWERL

Soil Texture	u_{*t} (m s^{-1}) Min. 2011	u_{*t} (m s^{-1}) Min. 2010	u_{*t} (m s^{-1}) Max. 2011	u_{*t} (m s^{-1}) Max. 2010	u_{*t} (m s^{-1}) Mean 2011	u_{*t} (m s^{-1}) Mean 2010	STD 2011	STD 2010	PI-SWERL Tests 2011	PI-SWERL Tests 2010
Loamy Sand	0.20	0.22	0.38	0.45	0.33	0.30	0.04	0.06	27	51
Sand	0.17	0.21	0.43	0.45	0.30	0.29	0.04	0.04	274	204
Sandy Loam	0.23	0.22	0.36	0.46	0.32	0.27	0.04	0.05	9	26
Silty Loam	0.25	0.34	0.39	0.47	0.34	0.43	0.05	0.05	6	15
Clay	N/A	0.46	N/A	0.47	N/A	0.47	N/A	0.01	N/A	5

Table 3.4 Analysis of variance between the threshold shear velocity (u*t) means grouped by surface soil texture (sig. 0.05).

Soil Texture	u_{*t} (m s^{-1}) Mean 2011	u_{*t} (m s^{-1}) Mean 2010	P-value
Loamy Sand	0.33	0.30	0.059
Sand	0.30	0.29	0.025
Sandy Loam	0.32	0.27	0.014
Silty Loam	0.34	0.43	0.003
		overall	8.4E-27

The lowest u_{*t} value for this field season, 0.17 ms^{-1}, was measured at a sand texture site and was used as the u_{*min} value in WE_DUST_EM. The minimum and mean u_{*t} values for each of the soil texture classes were used to generate a Gaussian distribution of values for each texture class within WE_DUST_EM. When the minimum threshold shear velocity for any hour modelled is exceeded a random value from within the Gaussian distribution of u_{*t} values for a soil class is assigned to a model grid cell and dust flux is calculated. Using a distribution rather than a fixed threshold shear velocity value for a soil texture class is done because field study tests show varying threshold shear velocity values within a given soil class. For example, sandy soils accounting for 76% of the study area have threshold shear velocity values from a low of 0.17 m s^{-1} to a maximum of 0.43 m s^{-1} with an average of 0.30 m s^{-1} (see Table 3.3). This variation in u_{*t}

within a soil texture class is due to the heterogeneity of the surface features controlling this important variable, such as surface crusting, particle size distribution, and the amount of loose material available at the surface.

When compared with u_{*t} values measured in 2010, there are several differences of note in the 2011 data set. First, although in both seasons the majority of the sites tested were at sand soil sites there was a lower representation of other soils classes in 2011, and no clay sites (Table 3.3). Overall, ANOVA analysis shows there is a significant statistical difference (at 0.05) in variance between the 2010 and 2011 u_{*t} with a p-value of 8.4E-27 (Table 1.4). When comparing the variance in u_{*t} between soil texture classes only loamy sand of the four was not statistically significant at 0.05 with a p-value of 0.059. The maximum u_{*t} values for the sand-texture soils is approximately the same for both seasons, but they were much higher in 2010 for remaining three soil classes (Table 3.3). For the silty loam soils the minimum u_{*t} was 0.34 m s^{-1} in the 2010 study, but was much lower in 2011 with a value of 0.25 m s^{-1}. Similarly, the mean u_{*t} values differ with 0.34 ms^{-1} in 2011 and 0.43 ms^{-1} in 2010. These differences will have a strong influence on the dust emission modelling as these u_{*t} values control whether or not sediment transport takes place and signals to the model whether or not to calculate dust emission. In particular, the lower minimum and mean u_{*t} for the silty loam soils will likely result in more frequent emission from these soils at a lower wind speed in 2011 than would have been predicted in the 2010 season.

Dust Flux

The relationship between the vertical dust flux (F, µg m^{-2} s^{-1}) and shear velocity (u_*, m s^{-1}) measured during the PI-SWERL tests show the expected power function form (Fig. 3.8). F is proportional to u_*^x with the values of x ranging from ≈1.5 to ≈4.7, which fall within the range of value cited for this relationship by Houser and Nickling (2001). The constants and exponents related to each PI-SWERL test site and related soil texture class are given in Fig. 3.8.

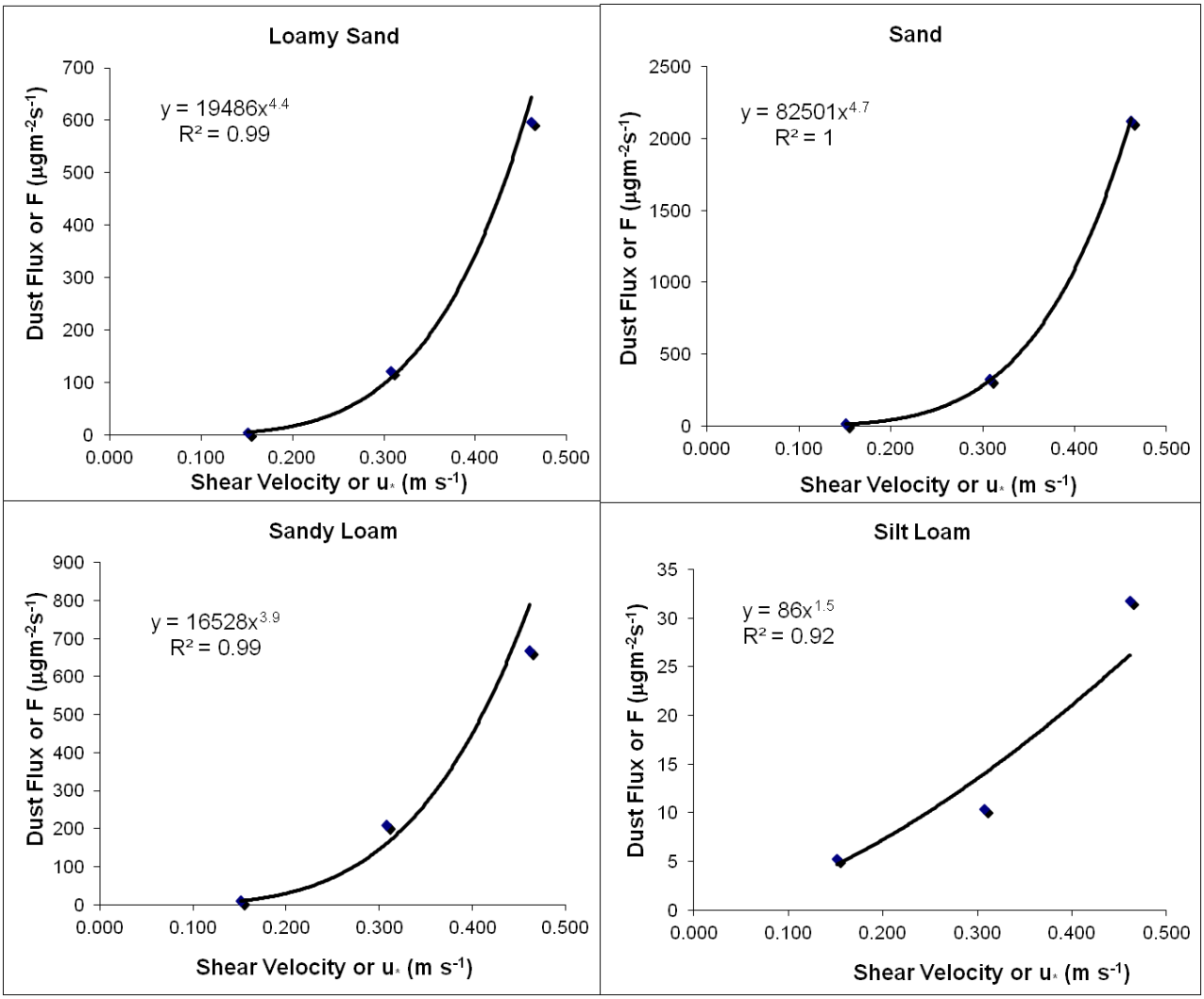

Figure 3.8 The relationships between vertical dust flux (F) and shear velocity (u*) for each soil texture category

3.3 Model Results

Potential dust emissions as a function of location for the Williston Reservoir beaches were modelled from May 20 to June 20, 2011. The WE_DUST_EM outputs have been mapped for all days and are provided in Appendix 1. To facilitate direct comparison with the output mapped for the 2010 field season a similar legend classification and colour scheme was used when mapping this season's model output. Overall, the dust emission values were lower for the 2011 season and therefore there is one less flux class in this year's maps. The very low wind speed on the dates of May 24, June 5, 12, and 16 resulted in surface shear velocity below threshold of 0.17 m s^{-1} and no dust emissions were generated by the model for these days. In contrast, June 13, 2011 and June 15, 2011 had the highest wind speeds and the highest daily dust emissions,

≈1475 and ≈1330 µg m^{-2} s^{-1}, respectively (Fig. 3.9). However, this year's values are much lower than highest daily emissions of ≈7,300 and ≈2,800 µg m^{-2} s^{-1} on May 24, 2010 and June 2, 2010. The higher winds of 2010 can be attributed to wind storms where high wind speeds persisted throughout the day, while during the 2011 field season high sustained winds were not observed. The high emissions of June 13, 2011 and June 2, 2010 are shown in Fig. 3.10, to illustrate some key points. Primarily, there is a similar pattern in both maps with the high emission beaches found in the Collins, Davis, Shovel, and Middle Creek sand texture soil areas. With the high sustained winds of 2010 almost all the beach is emitting, the only zero emissions area is a clay textured soil. The winds of 2011 do not generate dust emission from the southern section of the study area containing the sand textured beaches, which were active in 2010.

Figure 3.9. The highest modelled daily dust emission (F, µg m^{-2} s^{-1}) dates for the 2011 field season.

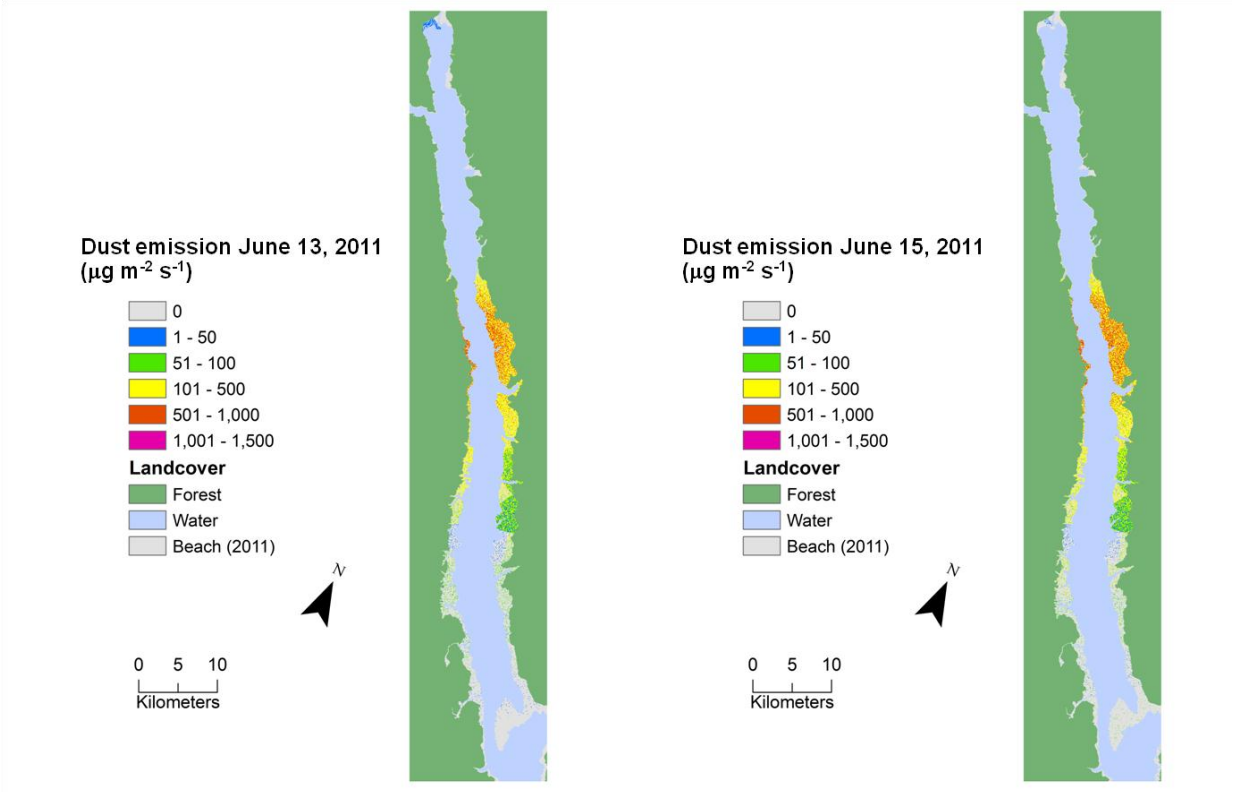

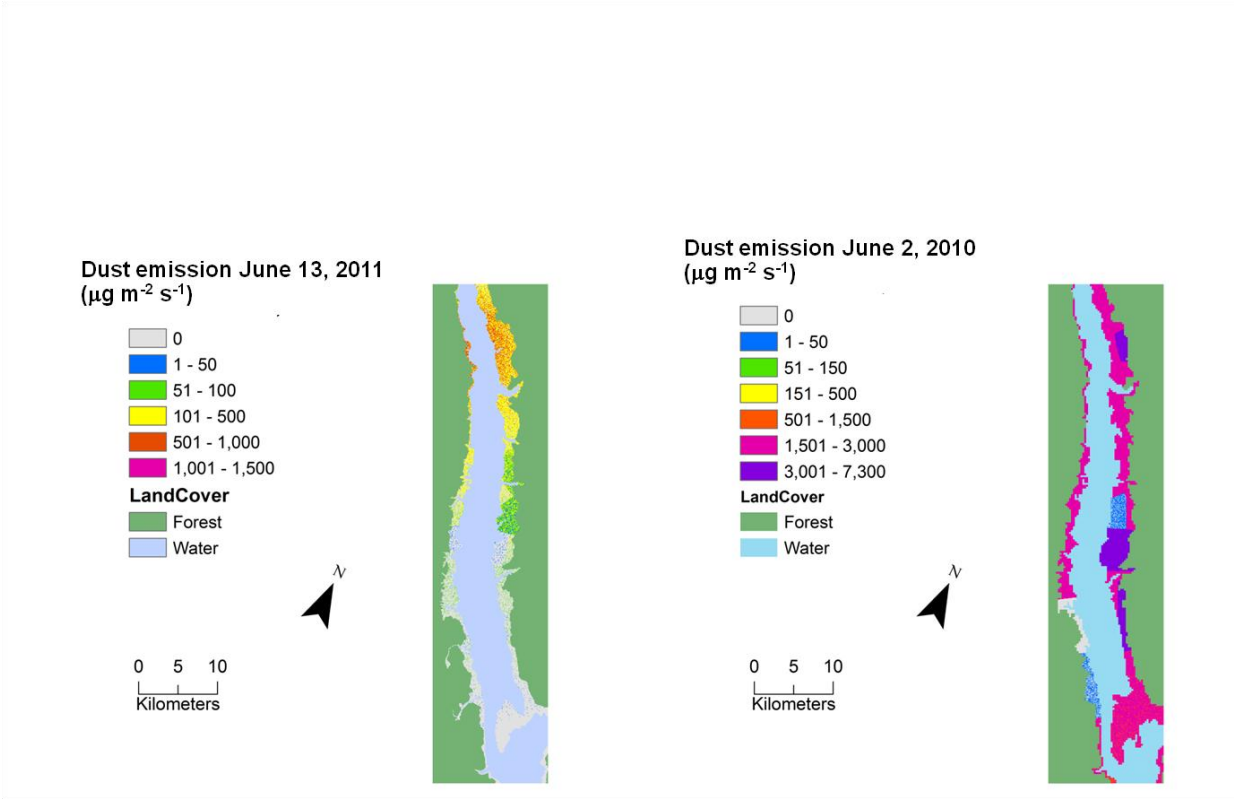

Figure 3.10. Comparison of highest modelled daily dust emission (F, µg m^{-2} s^{-1}) dates for 2010 and 2011 field seasons. The map for the 2011 field season has been clipped down to the extent of the 2010 season for this comparison.

Another difference between 2011 and 2010 is the extent of the study area with the inclusion of a site in the upper part of the study area, Tsay Keh. The soil samples collected during the PI-SWERL tests at the Tsay Keh site were determined to be a silty loam texture (Fig. 3.6). Of the 32 days modelled only 11 failed to have any emissions from the silty loam textured soils near Tsay Keh. Although the emissions were not high, the maximum value was ≈195 µg m^{-2} s^{-1} on June 8, 2011, this area did emit frequently (Fig. 3.11). As discussed in Section 3.2.2 the lower measured u_{*t} values in 2011 would likely result in more frequent emissions for this texture class.

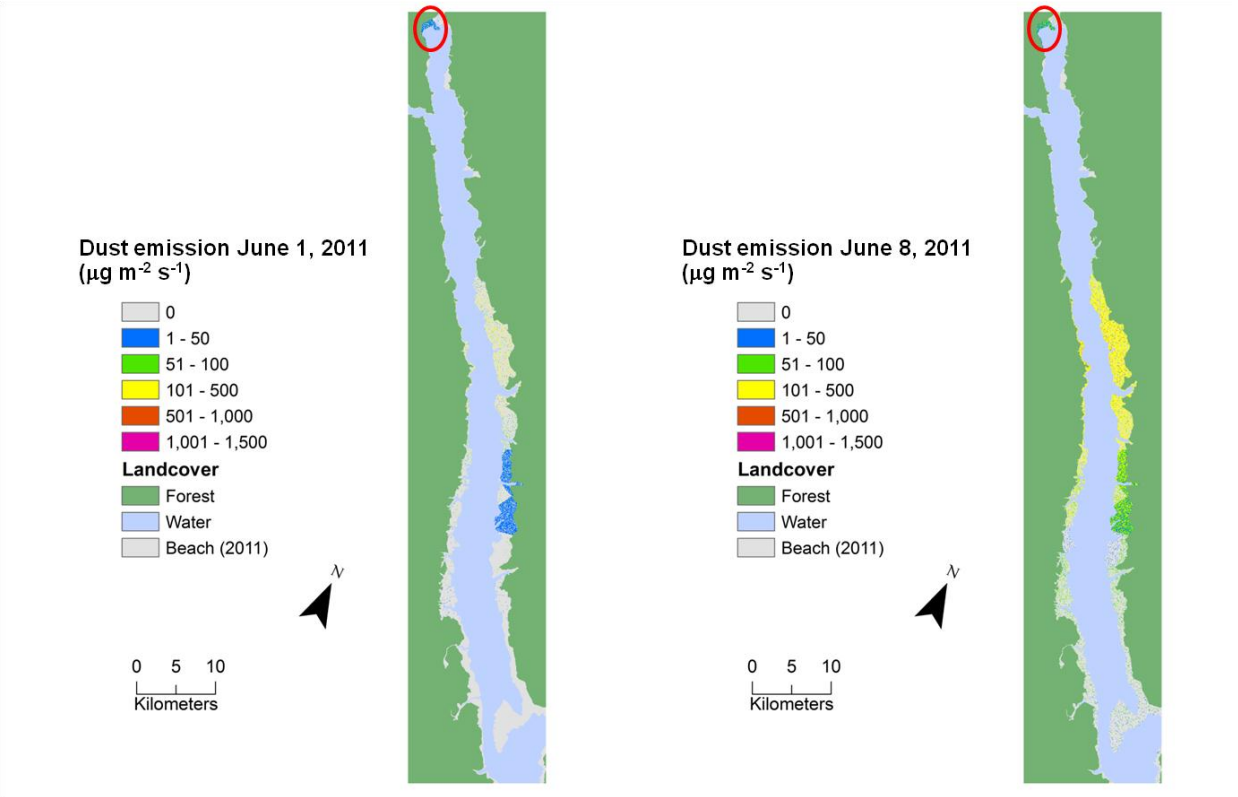

Figure 3.11. Examples of low level dust emissions (F, µg m^{-2} s^{-1}) at the top of study area, from the silty loam soils near the Tsay Keh PI-SWERL site.

3.4 CONCLUSIONS

This section has presented the WE_DUST_EM model and the dust emission potential of the beach surfaces for the modeled period for the 2011study. Overall, the modelled emission rates were lower for the 2011 season than they were for the 2010 season and support the results of the 2011 long term monitoring study. This can be attributed to the lack of sustained high wind speeds associated with storms, which occurred in 2010, but were not observed in the 2011 field season. There appears to be a consistent pattern of high emission beaches for the Collins, Davis, Shovel, and Middle Creek Sand areas. However, there are several key differences between the 2010 and 2011 seasons. The soil samples collected at the PI-SWERL test sites were primarily of a sand texture for both seasons, but in 2011 fewer test sites were of other textural classes. The textural class is unknown at the time of the PI-SWERL tests, but each year some tests are repeated in similar locations as 2010 and 2009, to evaluate how emissions vary through time for similar locations.

One key observation is that soil texture of beaches can change. Comparing the results of this year's textural analysis of repeat sites indicates that there are changes between years. For example, in 2010 there was an additional clay soil texture class and none of the test sites in 2010 were upon clay soils. Repeated testing of the same locations would confirm whether the surface soils change every year. The difference in soil texture classes affects the model results by affecting the spatial distribution of soil texture over the beach. It also means that there were fewer emissions data for the loamy sand, silty loam and sandy loam soils in 2011 upon which WE_DUST_EM relies for input data. The extension of the study area in 2011 to include the Tsay Keh site at the north end of the reservoir, revealed an area of beach that has frequent low-level dust emissions.

Further repeated PI-SWERL testing of the 2009, 2010 and 2011 sites is needed to confirm whether the emitting sites remain stable over time. This will provide valuable information to inform mitigation strategies, for example if they should be focused in s the same areas every dust emission season to more efficiently reduce the overall dust emission burden at the reservoir and the effect of this dust on air quality at the Tsay Keh village.

CITED REFERENCES

Brown, L. J. 2007. Wind erosion in sparsely vegetated rangelands PhD. University of Guelph, Guelph. 174 pp.

Et

Fryrear, D. W., Bilbro, J. D., Saleh, A., Schomberg, H., Stout, J. E. and Zobeck, T. M. 2000. RWEQ: Improved Wind Erosion Technology. Journal of Soil and Water Conservation 55(2):183-189.

Fryrear, D. W., Sutherland, P. L., Davis, G., Hardee, G. and Dollar, M. 1999. Wind erosion estimates with RWEQ and WEQ. Proc. Sustaining the Global Farm: Selected Papers from the 10th International Soil Conservation Organization Meeting, Purdue University and USDA-ARS National Soil Research Laboratory.

Gillette, D. A. 1979. Environmental factors affecting dust emissions by wind erosion. Pages 71-94 *in* C. Morales, ed. Saharan Dust. John Wiley, New York.

Gillette, D. A., Adams, J., Endo, A., Smith, D. and Kihl, R. 1980. Threshold velocities for input of soil particles into the air by desert soils. Journal of Geophysical Research 85(C10):5621-5630.

Gillette, D. A. and Passi, R. 1988. Modelling dust emission caused by wind erosion. Journal of Geophysical Research 93(D11):14,233-14,242.

Gillies, J.A. (2012). Fundamentals of aeolian sediment transport | dust emissions and transport – near surface. In *Treatise on Geomorphology*, Shroder, J. (ed. in chief) and Lancaster, N. (ed.), Academic Press, San Diego, CA, vol. 11, pp. xx-xx (in press).

Houser, C. A. and Nickling, W. G. 2001. The Emission and Vertical Flux of Particulate Matter <10 µm from a Disturbed Clay-Crusted Surface. Sedimentology 48:255-267.

Lillesand, T. M. and Kiefer, R. W. (2000). Remote Sensing and Image Interpretation. 4 ed. John Wiley & Sons, Inc. , New York.

Marticorena, B. and Bergametti, G. 1995. Modeling the atmospheric dust cycle:1. Design of a soil-derived dust emission scheme. Journal of Geophysical Research 100(D8):16415-16430.

Marticorena, B., Bergametti, G., Aumont, B., Callot, Y., N'Doume, C. and Legrand, M. 1997. Modelling the atmospheric dust cycle 2. Simulation of Saharan dust sources. Journal of Geophysical Research 102(D4):4387-4404.

McKenna Neuman, C., and W. G. Nickling (1989), A theoretical and wind tunnel investigation of the effect of capillary water on the entrainment of sediment by wind, *Canadian Journal of Soil Science*, *69*(1), 79-96.

Nickling, W. G., Gillies, J., Brown, L. J. and Trant, J. 2011. A Feasibility Study for the Development of a RADARSAT-2 Dust Prediction System: 2010 Final Report.

Ravi, S., and P. D'Odorico (2005), A field-scale analysis of the dependence of wind erosion threshold velocity on air humidity, *Geophysical Research Letters*, *32*(L21404).

Ravi, S., P. D'Odorico, T. M. Over, and T. M. Zobeck (2004), On the effect of air humidity on soil susceptibility to wind erosion: The case of air-dry soils, *Geophysical Research Letters*, *31*(L09501).

Shao, Y. (2000), *Physics and Modelling of Wind Erosion*, 393 pp., Kluwer Academic Publishers, Dordrecht.

Shao, Y. (2004), Simplification of a dust emission scheme and comparison with data, *Journal of Geophysical Research*, *109*(D10202), doi:10.1029/2003JD004372.

von Kármán, T. 1954. Aerodynamics. Cornell University Press, Ithaca. 203 pp.

APPENDIX 1

The complete set of mapped WE_DUST_EM output for the 2011 season dates modeled May 20 through to June 20. Units of PM_{10} daily dust emission (F) classes are in $\mu g\ m^{-2}\ s^{-1}$.

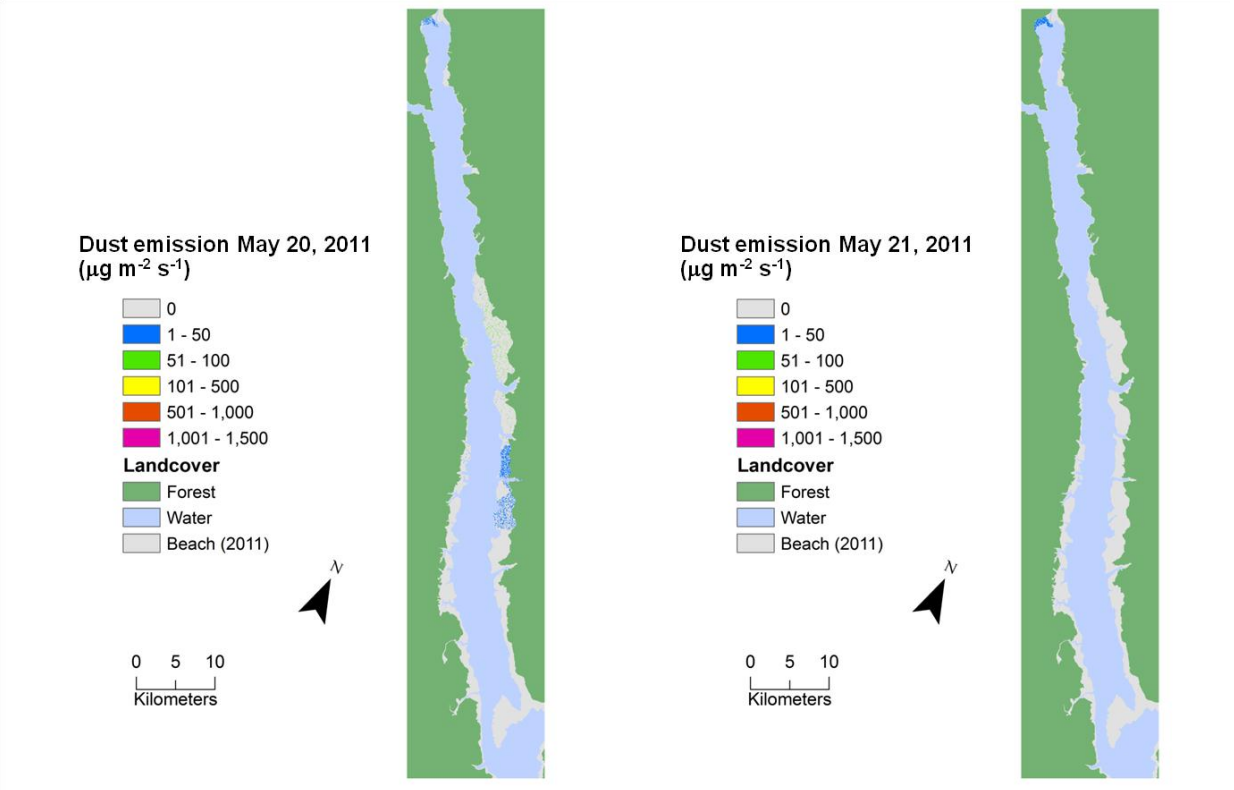

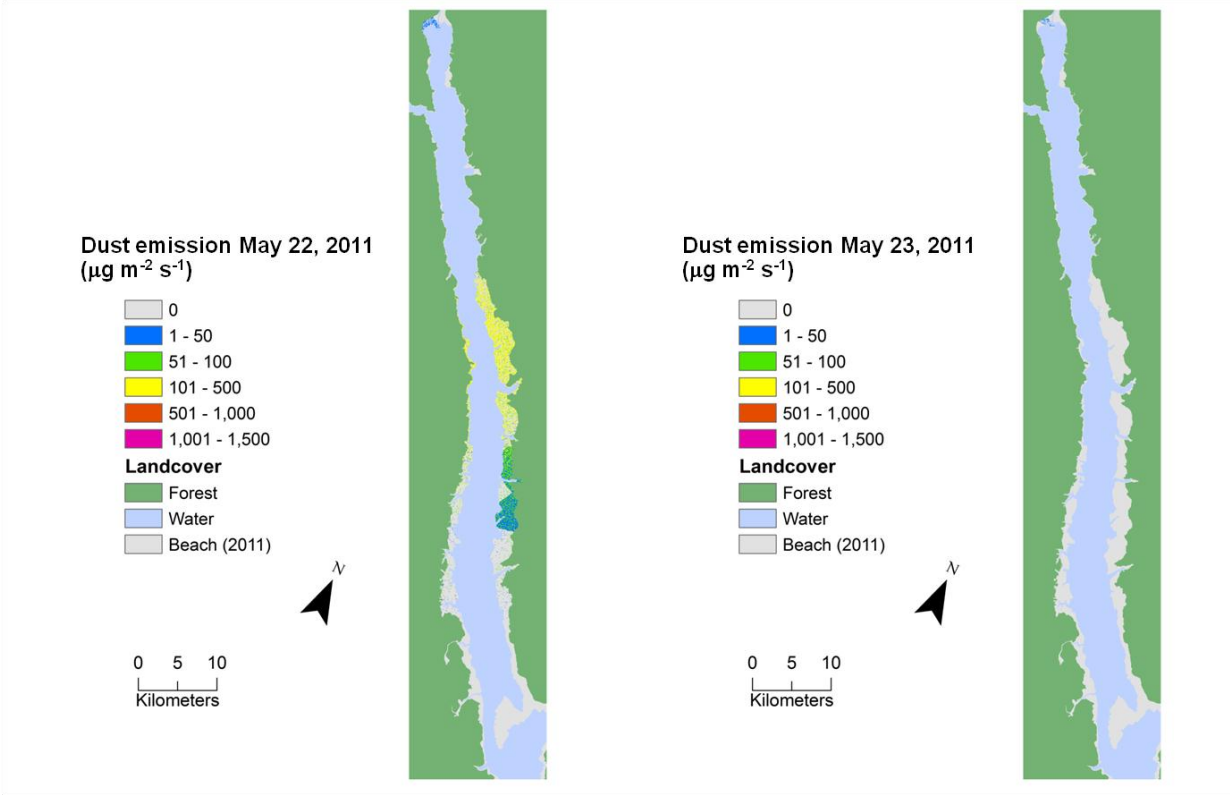
Dust emission May 22, 2011
(µg m-2 s-1)
0
1 - 50
51 - 100
101 - 500
501 - 1,000
1,001 - 1,500
Landcover
Forest
Water
Beach (2011)
N
0 5 10
Kilometers
Dust emission May 23, 2011
(µg m-2 s-1)
0
1 - 50
51 - 100
101 - 500
501 - 1,000
1,001 - 1,500
Landcover
Forest
Water
Beach (2011)
N
0 5 10
Kilometers

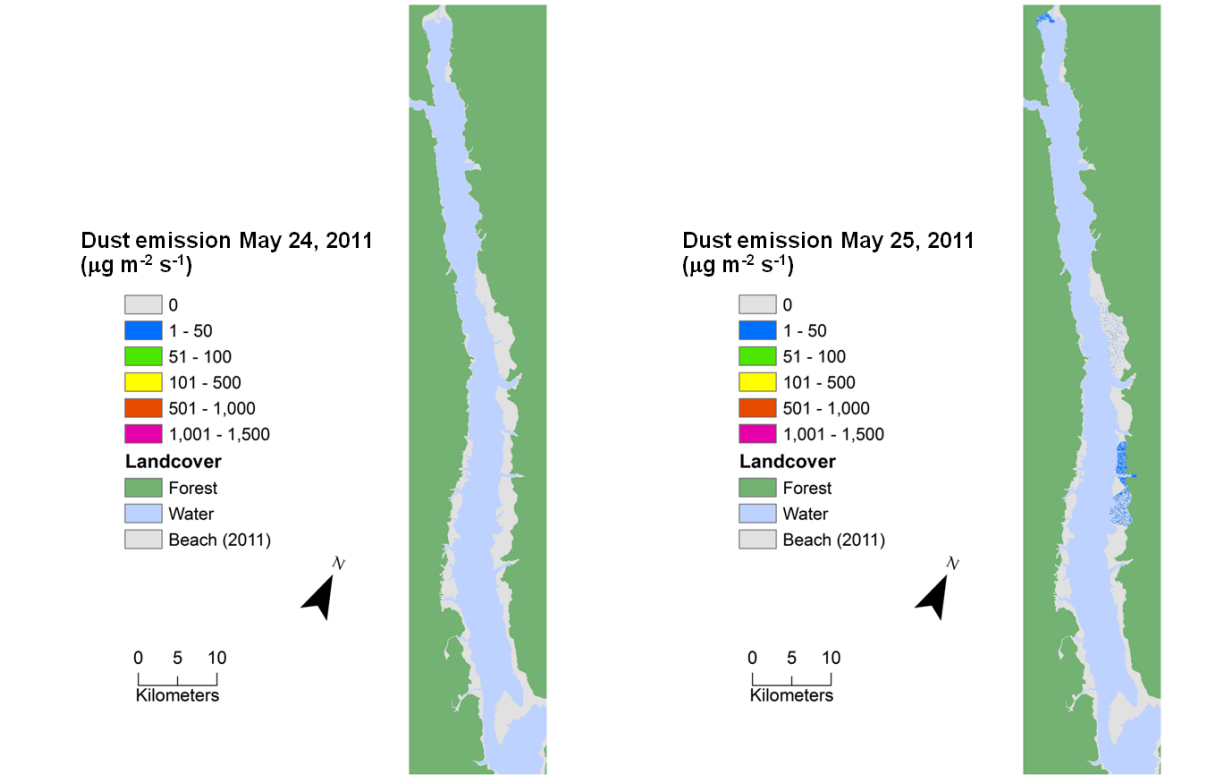
Dust emission May 24, 2011
(µg m-2 s-1)
0
1 - 50
51 - 100
101 - 500
501 - 1,000
1,001 - 1,500
Landcover
Forest
Water
Beach (2011)
N
0 5 10
Kilometers
Dust emission May 25, 2011
(µg m-2 s-1)
0
1 - 50
51 - 100
101 - 500
501 - 1,000
1,001 - 1,500
Landcover
Forest
Water
Beach (2011)
N
0 5 10
Kilometers

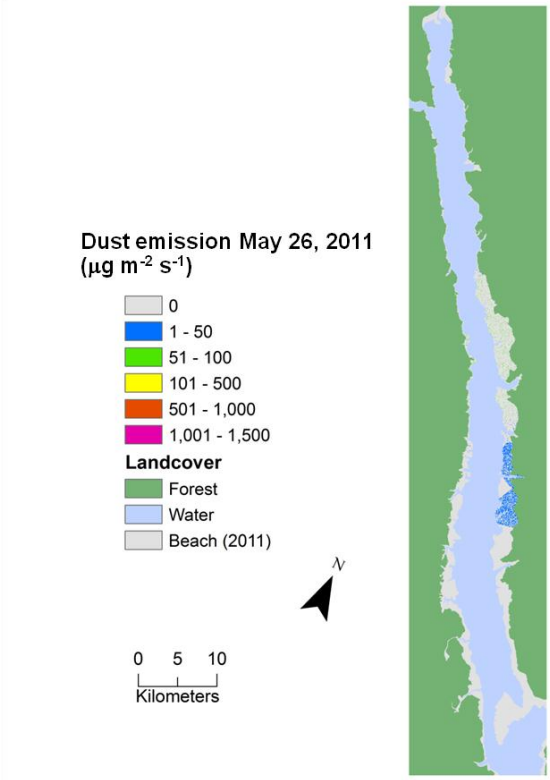
Dust emission May 26, 2011
(µg m-2 s-1)
0
1 - 50
51 - 100
101 - 500
501 - 1,000
1,001 - 1,500
Landcover
Forest
Water
Beach (2011)
N
0 5 10
Kilometers

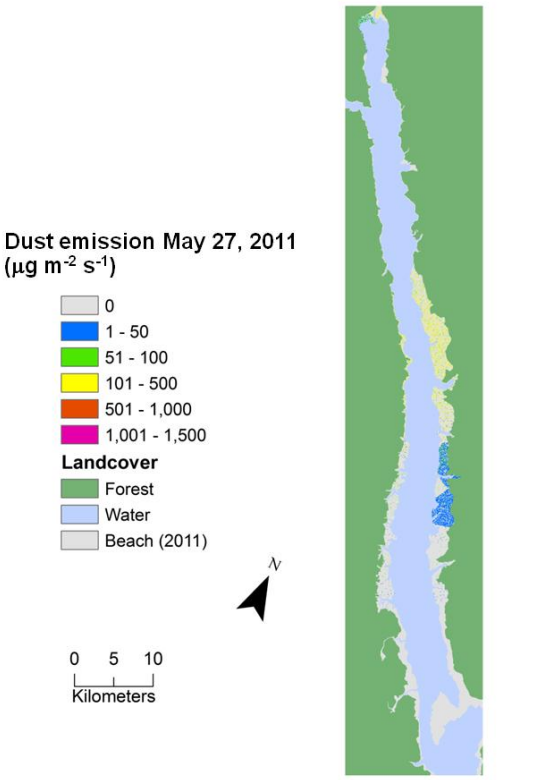
Dust emission May 27, 2011
(µg m-2 s-1)
0
1 - 50
51 - 100
101 - 500
501 - 1,000
1,001 - 1,500
Landcover
Forest
Water
Beach (2011)
N
0 5 10
Kilometers

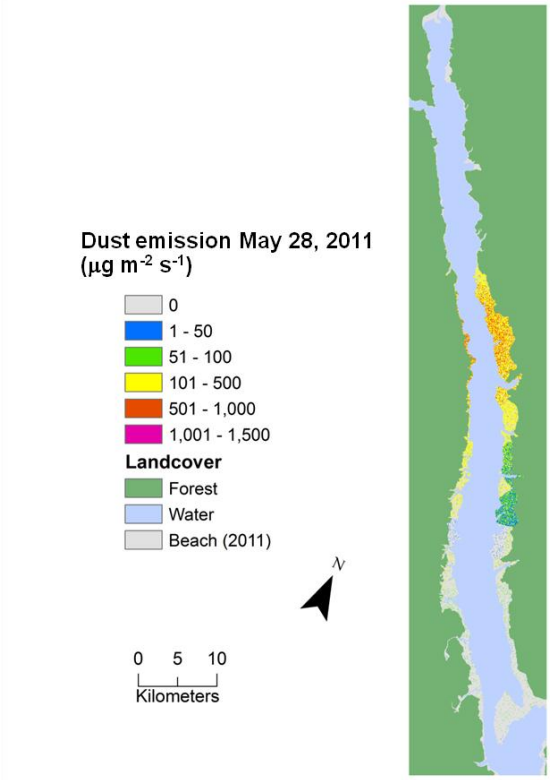
Dust emission May 28, 2011
(µg m-2 s-1)
0
1 - 50
51 - 100
101 - 500
501 - 1,000
1,001 - 1,500
Landcover
Forest
Water
Beach (2011)
N
0 5 10
Kilometers

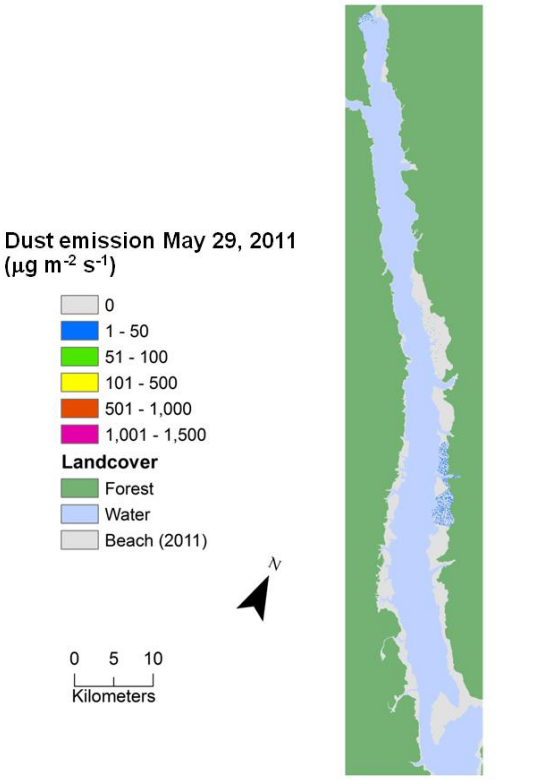
Dust emission May 29, 2011
(µg m-2 s-1)
0
1 - 50
51 - 100
101 - 500
501 - 1,000
1,001 - 1,500
Landcover
Forest
Water
Beach (2011)
N
0 5 10
Kilometers

Dust emission May 30, 2011
(µg m^{-2} s^{-1})

0
1 - 50
51 - 100
101 - 500
501 - 1,000
1,001 - 1,500

Landcover

Forest
Water
Beach (2011)

N

0 5 10
Kilometers

Dust emission May 31, 2011
(µg m^{-2} s^{-1})

0
1 - 50
51 - 100
101 - 500
501 - 1,000
1,001 - 1,500

Landcover

Forest
Water
Beach (2011)

N

0 5 10
Kilometers

Dust emission June 1, 2011
(µg m^{-2} s^{-1})

0
1 - 50
51 - 100
101 - 500
501 - 1,000
1,001 - 1,500

Landcover

Forest
Water
Beach (2011)

N

0 5 10
Kilometers

Dust emission June 2, 2011
(µg m^{-2} s^{-1})

0
1 - 50
51 - 100
101 - 500
501 - 1,000
1,001 - 1,500

Landcover

Forest
Water
Beach (2011)

N

0 5 10
Kilometers

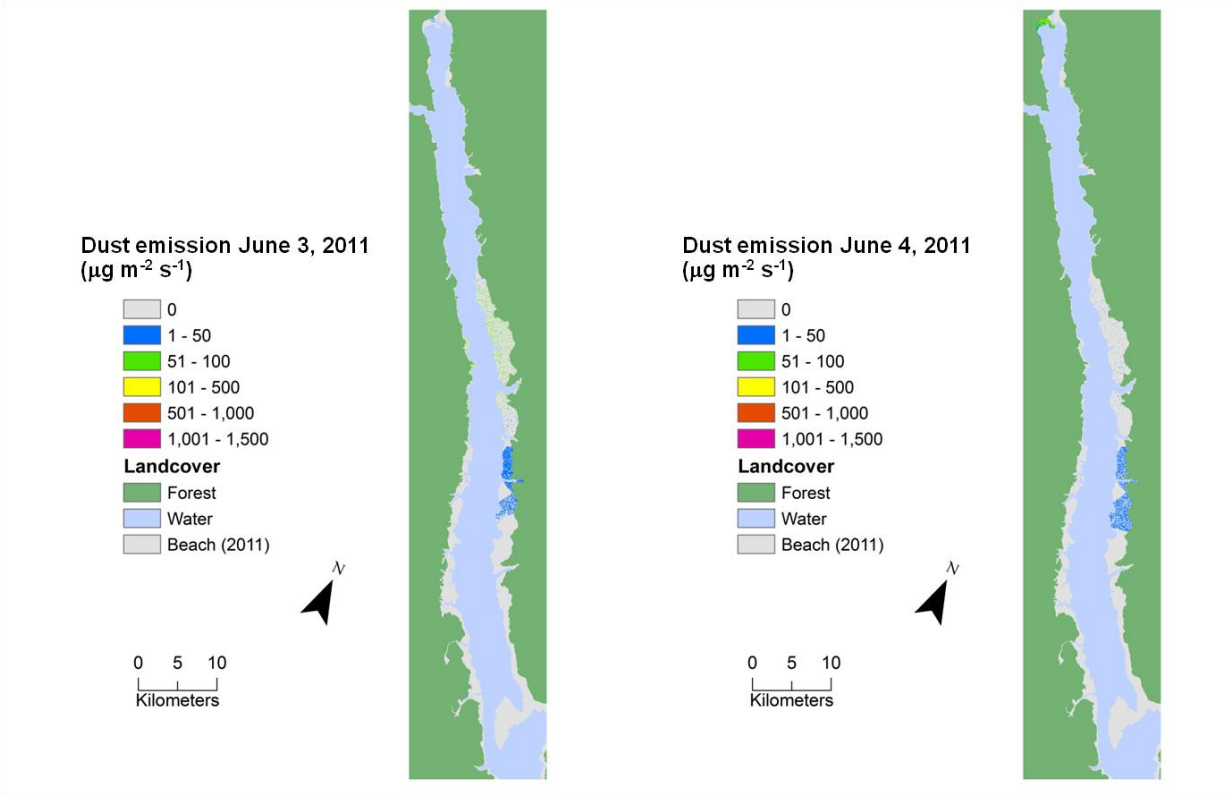
Dust emission June 3, 2011
(µg m-2 s-1)
0
1 - 50
51 - 100
101 - 500
501 - 1,000
1,001 - 1,500
Landcover
Forest
Water
Beach (2011)
N
0 5 10
Kilometers
Dust emission June 4, 2011
(µg m-2 s-1)
0
1 - 50
51 - 100
101 - 500
501 - 1,000
1,001 - 1,500
Landcover
Forest
Water
Beach (2011)
N
0 5 10
Kilometers

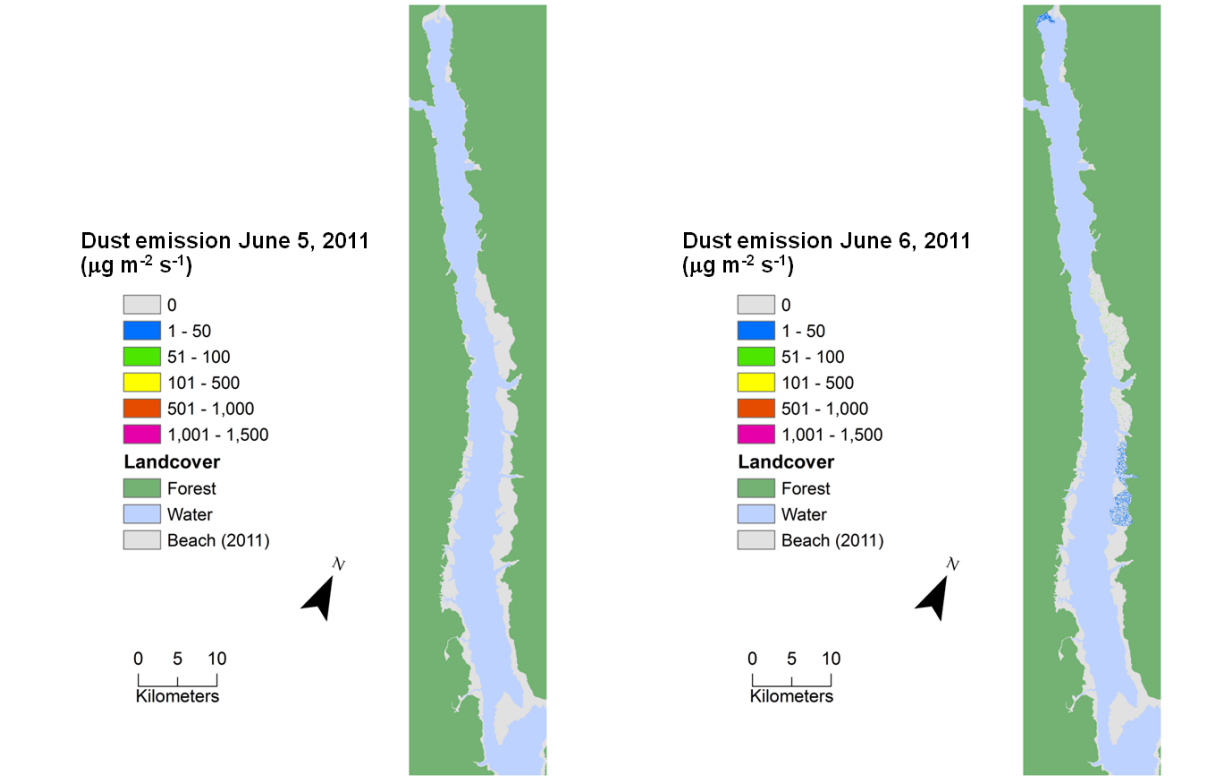
Dust emission June 5, 2011
(µg m-2 s-1)
0
1 - 50
51 - 100
101 - 500
501 - 1,000
1,001 - 1,500
Landcover
Forest
Water
Beach (2011)
N
0 5 10
Kilometers
Dust emission June 6, 2011
(µg m-2 s-1)
0
1 - 50
51 - 100
101 - 500
501 - 1,000
1,001 - 1,500
Landcover
Forest
Water
Beach (2011)
N
0 5 10
Kilometers

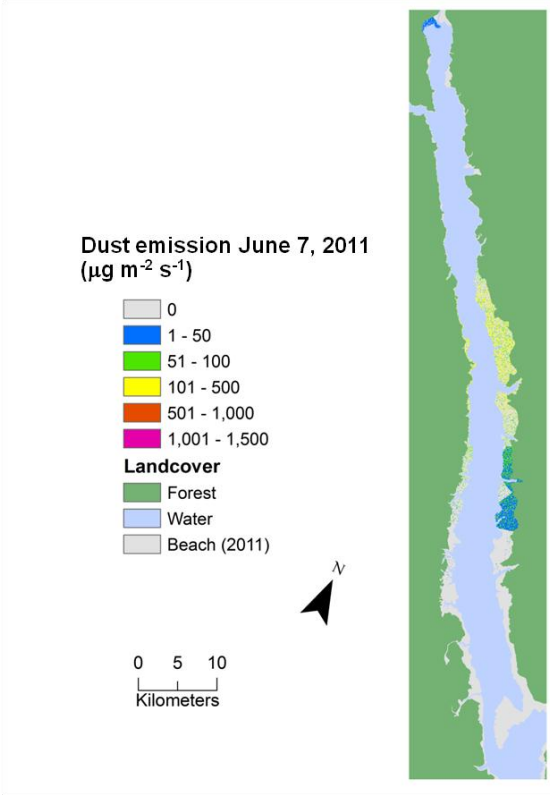
Dust emission June 7, 2011
(µg m-2 s-1)
0
1 - 50
51 - 100
101 - 500
501 - 1,000
1,001 - 1,500
Landcover
Forest
Water
Beach (2011)
N
0 5 10
Kilometers

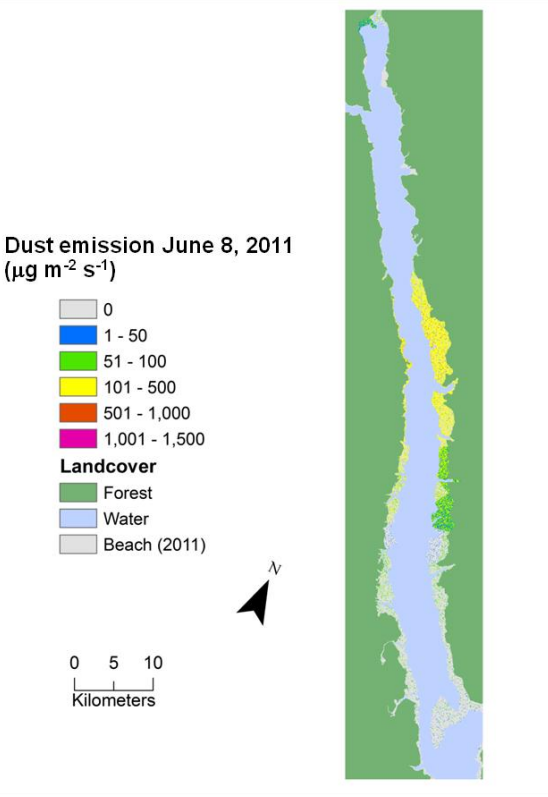
Dust emission June 8, 2011
(µg m-2 s-1)
0
1 - 50
51 - 100
101 - 500
501 - 1,000
1,001 - 1,500
Landcover
Forest
Water
Beach (2011)
N
0 5 10
Kilometers

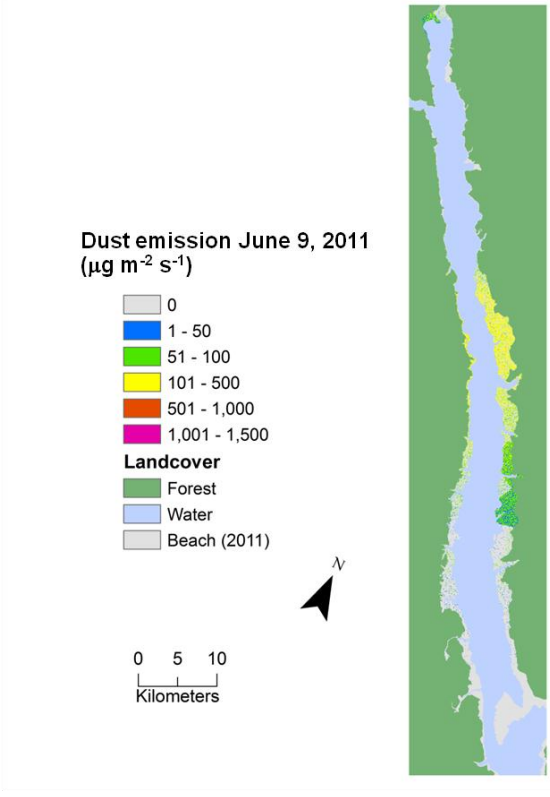
Dust emission June 9, 2011
(µg m-2 s-1)
0
1 - 50
51 - 100
101 - 500
501 - 1,000
1,001 - 1,500
Landcover
Forest
Water
Beach (2011)
N
0 5 10
Kilometers

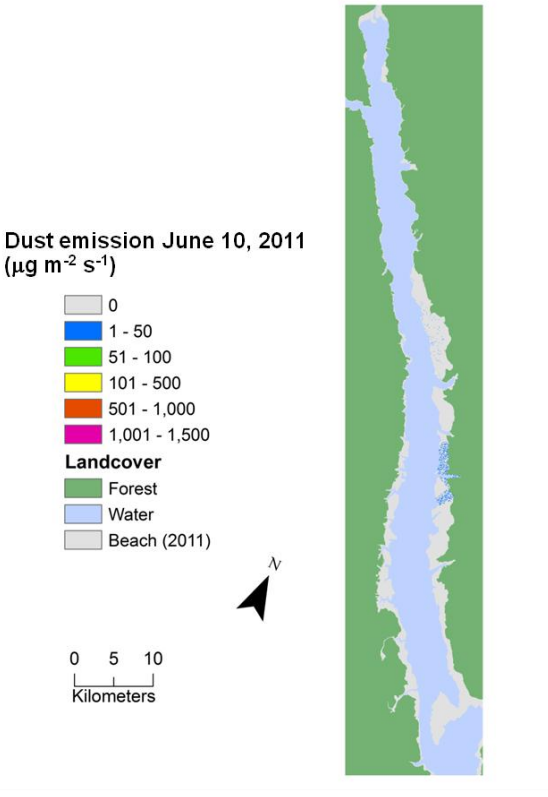
Dust emission June 10, 2011
(µg m-2 s-1)
0
1 - 50
51 - 100
101 - 500
501 - 1,000
1,001 - 1,500
Landcover
Forest
Water
Beach (2011)
N
0 5 10
Kilometers

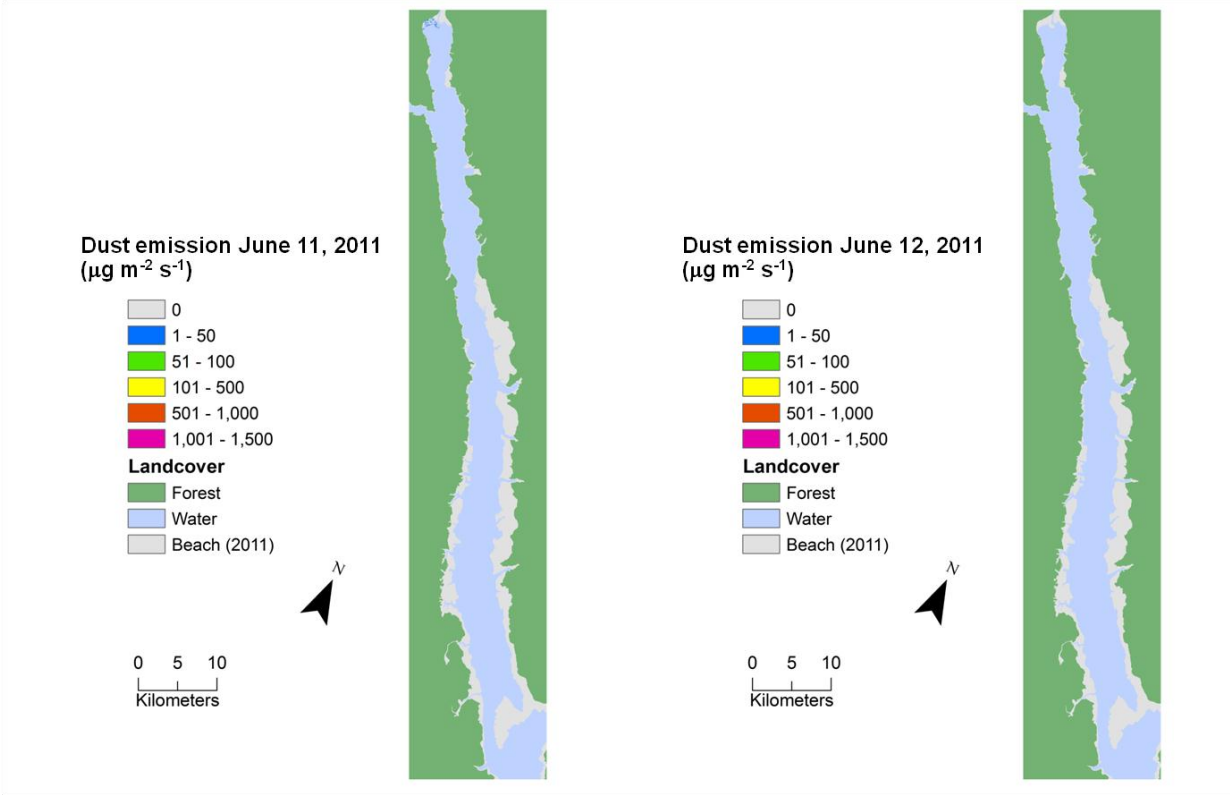
Dust emission June 11, 2011
(µg m-2 s-1)
0
1 - 50
51 - 100
101 - 500
501 - 1,000
1,001 - 1,500
Landcover
Forest
Water
Beach (2011)
N
0 5 10
Kilometers
Dust emission June 12, 2011
(µg m-2 s-1)
0
1 - 50
51 - 100
101 - 500
501 - 1,000
1,001 - 1,500
Landcover
Forest
Water
Beach (2011)
N
0 5 10
Kilometers

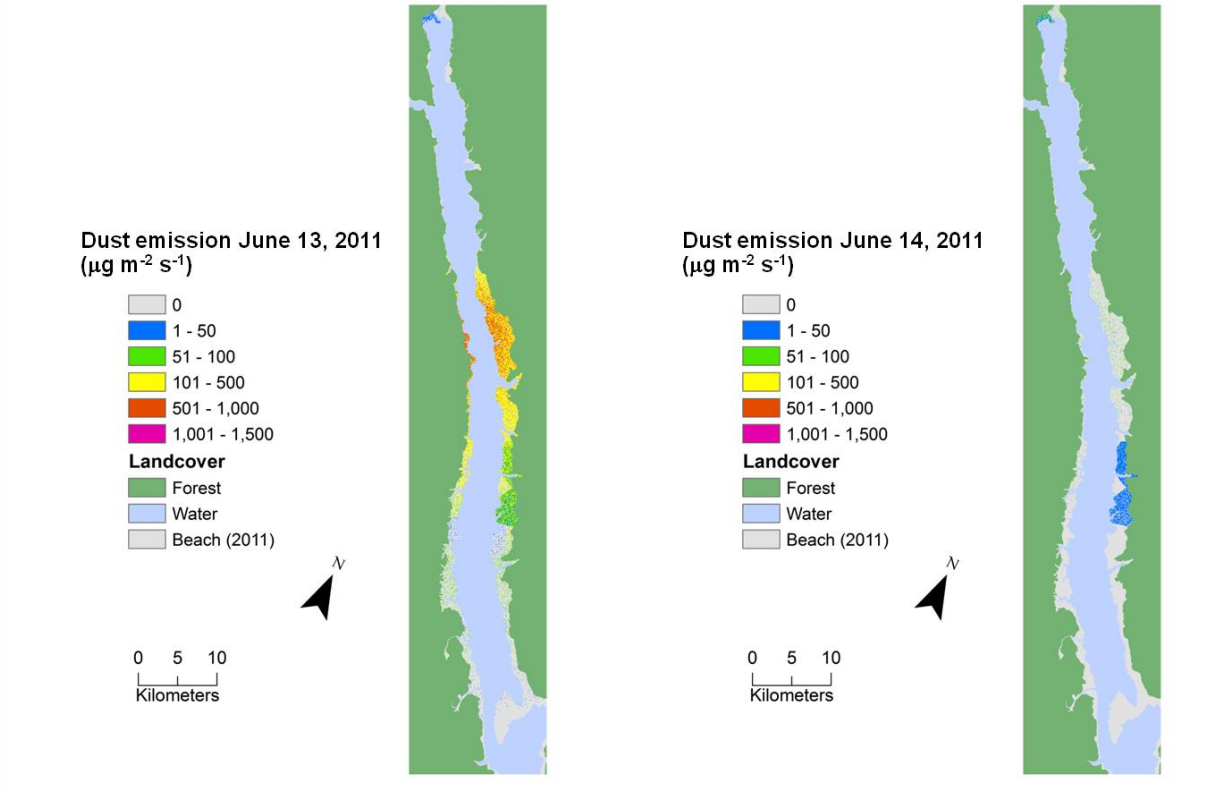
Dust emission June 13, 2011
(µg m-2 s-1)
0
1 - 50
51 - 100
101 - 500
501 - 1,000
1,001 - 1,500
Landcover
Forest
Water
Beach (2011)
N
0 5 10
Kilometers
Dust emission June 14, 2011
(µg m-2 s-1)
0
1 - 50
51 - 100
101 - 500
501 - 1,000
1,001 - 1,500
Landcover
Forest
Water
Beach (2011)
N
0 5 10
Kilometers

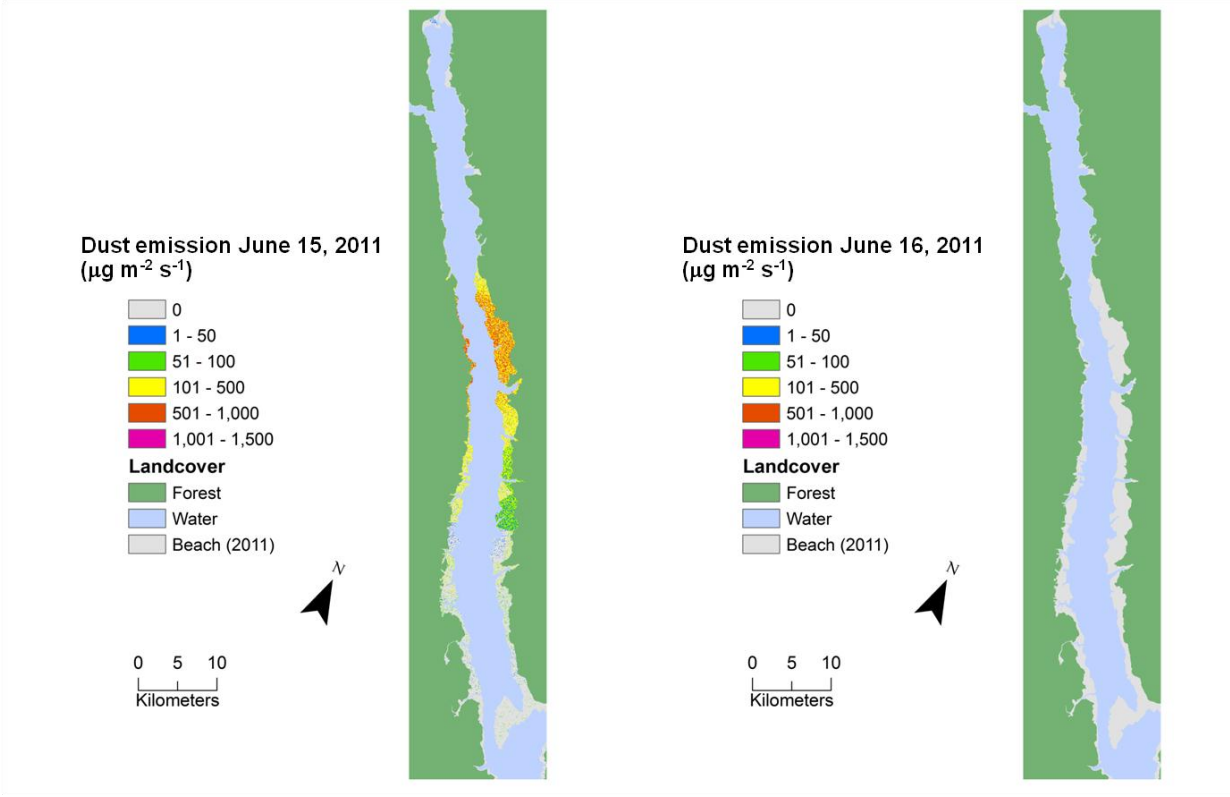
Dust emission June 15, 2011
(µg m-2 s-1)
0
1 - 50
51 - 100
101 - 500
501 - 1,000
1,001 - 1,500
Landcover
Forest
Water
Beach (2011)
N
0 5 10
Kilometers
Dust emission June 16, 2011
(µg m-2 s-1)
0
1 - 50
51 - 100
101 - 500
501 - 1,000
1,001 - 1,500
Landcover
Forest
Water
Beach (2011)
N
0 5 10
Kilometers

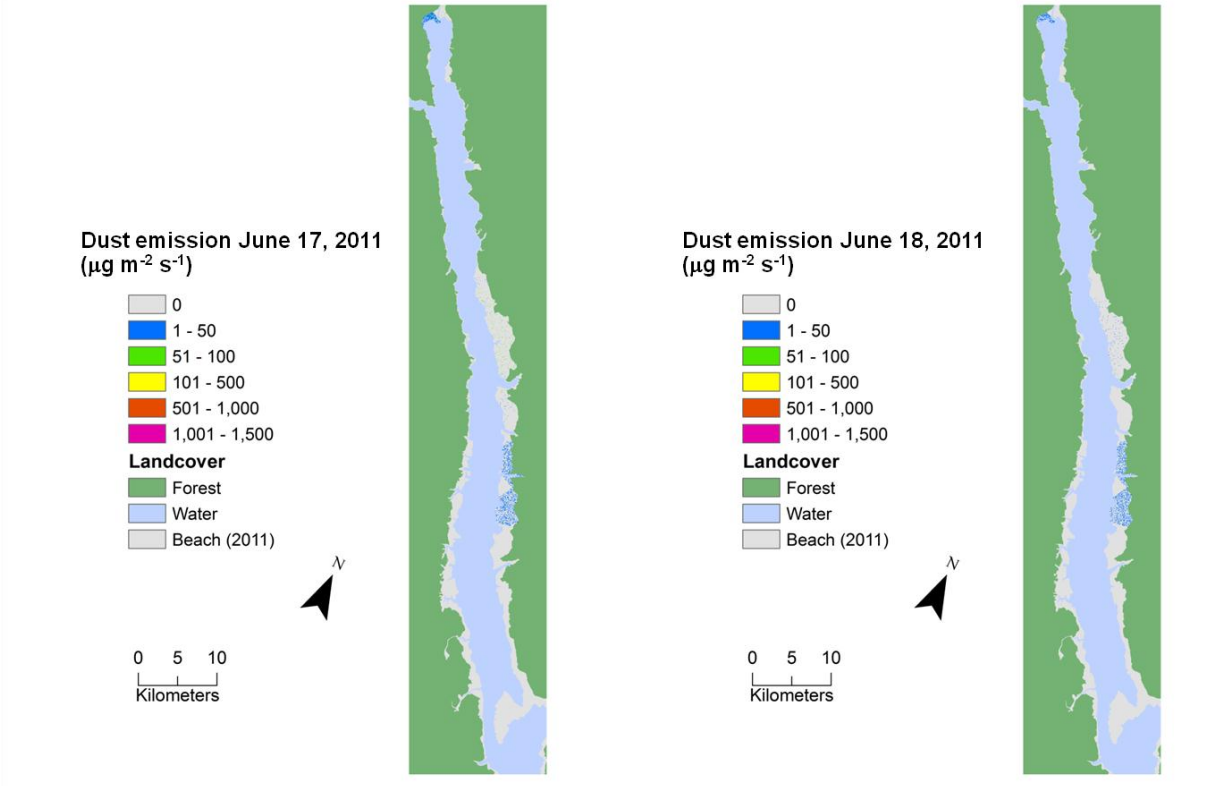
Dust emission June 17, 2011
(µg m-2 s-1)
0
1 - 50
51 - 100
101 - 500
501 - 1,000
1,001 - 1,500
Landcover
Forest
Water
Beach (2011)
N
0 5 10
Kilometers
Dust emission June 18, 2011
(µg m-2 s-1)
0
1 - 50
51 - 100
101 - 500
501 - 1,000
1,001 - 1,500
Landcover
Forest
Water
Beach (2011)
N
0 5 10
Kilometers

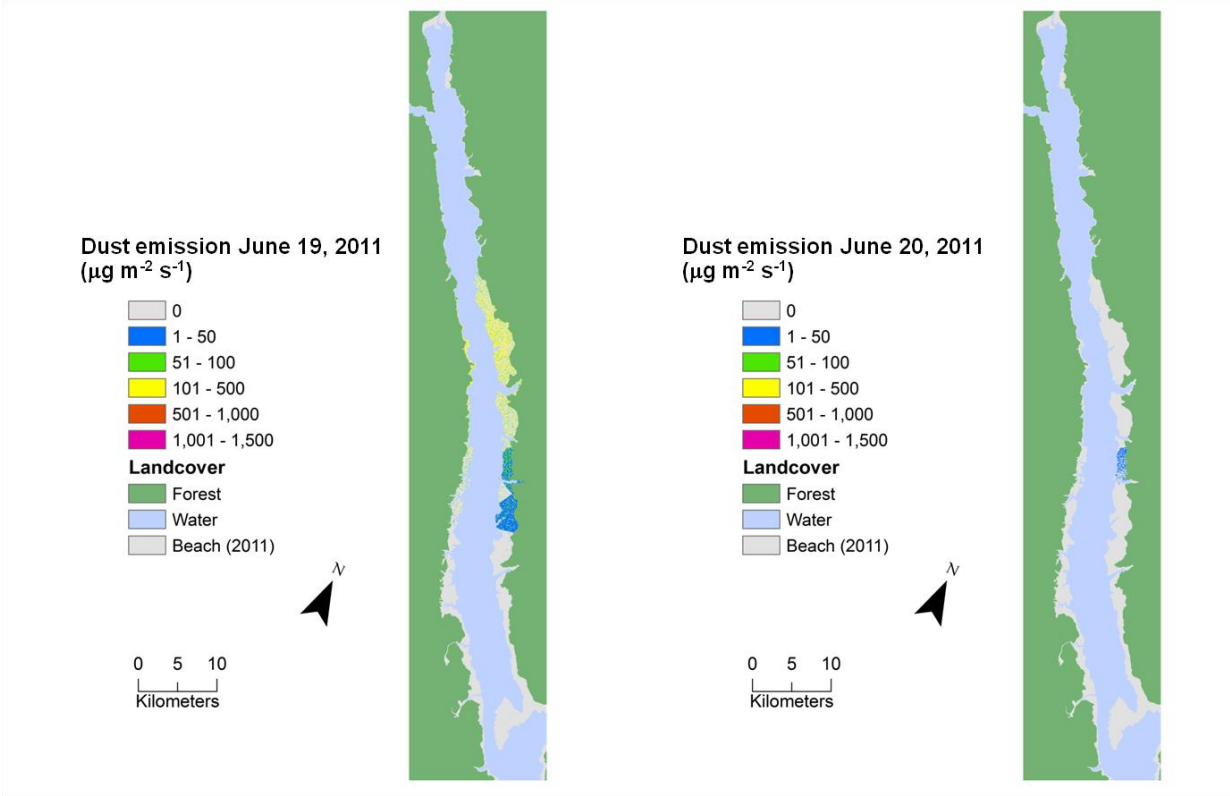
Dust emission June 19, 2011
(μg m-2 s-1)
0
1 - 50
51 - 100
101 - 500
501 - 1,000
1,001 - 1,500
Landcover
Forest
Water
Beach (2011)
N
0 5 10
Kilometers
Dust emission June 20, 2011
(μg m-2 s-1)
0
1 - 50
51 - 100
101 - 500
501 - 1,000
1,001 - 1,500
Landcover
Forest
Water
Beach (2011)
N
0 5 10
Kilometers

APPENDIX 2

The Wind Erosion Dust Emission model (WE_DUST_EM copyright 2011) formerly known as the DUST_EM model was developed as a tool to spatially and temporally distribute empirically derived wind erosion and dust emission relationships (Brown 2007). The model's algorithms are based on observations made during the field research, and the models and equations reported in the aeolian literature. Numerical wind erosion and dust emission models calculate soil loss by numerically simulating the processes involved in wind erosion and dust emission. Wind erosion and dust emission models incorporate the many sub-processes of wind erosion into one model. Two approaches are used to numerically describe these sub-processes, empirically based models and physically-based process-based models, however many models incorporate a combination of these two approaches. The Revised Wind Erosion Equation (RWEQ) is an example of a model that combines these two approaches to model soil loss from agricultural soils (Fryrear et al. 2000; Fryrear et al. 1999). One of the limitations of this model are the empirically based components which are derived from agricultural soils. This means that an application outside of the agricultural context will compromise the results. An advantage of physically-based process models is their transferability. An example of a process-based model is Marticorena and Bergametti's (1995; Marticorena et al. 1997) macroscale dust emission model. However, it too has incorporated some empirically based aspects in its structure. For example, dust flux in the Marticorena and Bergametti (1995; Marticorena et al. 1997) model is the averaged ratio of dust flux (F) to sand flux (q) combined with the clay content of the soil based on Gillette's (1979) data set. One of the disadvantages of a process-based modelling approach involves the extensive data demand. Since each sub-process is numerically computed, complete detailed and accurate data sets for each input parameter are required. In reality these data sets are difficult if not impossible to obtain, or may not accurately represent the surface being modelled. By contrast, empirical relationships incorporate some of these sub-processes and are generally less data intensive.

The WE_DUST_EM model is a mesoscale wind erosion dust emission developed for applications outside of the agricultural context, incorporating stochastic methods and both empirical and process-based approaches. WE_DUST_EM is programmed in FORTRAN 90 and utilizes equations that describe 1) the force of the wind at the surface and 2) the vertical dust emissions. It is the shear stress at the surface, which is responsible for the detachment, and entrainment of soil particles. The surface shear stress ($\tau 0$) is related to the shear velocity (u^*) by:

$$u_* = \sqrt{\frac{\tau_o}{\rho_a}}$$

where ρ_a is air density. Therefore, an increase in wind speed increases the u_*, which in turn increases the shear stress on a bare surface. Once the shear stress at the surface is strong enough to overcome the resisting forces of that surface, sediment begins to move and the threshold shear velocity (u_{*t}) has been reached. The first equation used in WE_DUST_EM is one that can calculate shear velocity of a bare surface, the Prandtl- von Karman equation:

$$\frac{u_z}{u_*} = \frac{1}{\kappa} ln\left(\frac{z}{z_o}\right)$$

where u_z (m s^{-1}) is the wind speed at height z (m), κ is von Karman's constant (0.4), z_0 (m) is the aerodynamic roughness length, and u_* (m s^{-1}) is the shear velocity. Once threshold shear velocity has been exceeded, the relationship between dust emission (or vertical dust flux, F) and surface shear velocity (u_*) is best described by a power function where F is proportional to u_*. Therefore, dust flux can be calculated by:

$$F=Cu_*^{xsoil}$$

where: F is dust flux (µg m^{-2} s^{-1}), C is the constant related to a given soil texture class, u_* is shear velocity (m s^{-1}) and xsoil is the exponent related to the soil texture class.

A key parameter used in WE_DUST_EM to estimate wind erosion and/or dust emission is the minimum wind force needed to initiate particle movement, known as the threshold shear velocity (u_{*t}) for that surface. Threshold shear velocity is an important parameter since it defines the moment soil erosion is initiated. In this model a range of threshold shear velocity values for a bare soil texture class are used based on the empirical observations made at the study site. Basic descriptive statistics including, the minimum, mean and standard deviation for the range of threshold shear velocity values of a soil texture, are used to generate a Gaussian distribution. Stochasticity is incorporated into the model's structure when a random variable is drawn from this distribution and is subsequently used to define the threshold shear velocity for the soil within a model grid cell. By using empirically based values instead of using a processed-based approach to modelling a soil's threshold shear velocity all the factors influencing this parameter are implicitly incorporated. These factors include, microscale roughness, soil aggregation such as clods or crusts, and soil moisture. Because these factors vary temporally and spatially, a stochastic approach is used to account for this heterogeneity and uncertainty. Other factors of the surface not specifically addressed in this model are the evolution of the surface during a wind erosion event. This model assumes a limitless supply of loose material at the surface and does not account for the possible depletion of these particles over time.

WE_DUST_EM is a physically-based distributed model which captures spatial heterogeneity by placing a grid over the study area and parameter and variable data are input for each grid cell.

Furthermore, spatial variability within a grid cell can be captured by dividing the grid cell into subareas, each with its own parameter set. Subareas within a grid cell are characterized by homogeneity of several parameters. The modeller defines the size of grid cells and whether or not to the surface warrants further divisions into subareas (note: for the Williston beaches the surface is relatively homogenous therefore the model grid cells are not subdivided). Each grid cell can have up to 5 subareas. Four basic input data types are need for the model: 1) 10m wind speeds for each grid cell 2) surface attributes (e.g. soil texture and roughness length) for each subarea 3) threshold shear velocity for each soil texture and 4) dust flux data for each soil texture (Table A1). Of the four data types one is a variable, 10m wind speed and the rest are parameters. Most of the parameters are hard coded into the WE_DUST_EM model when the code is compiled as a 'parameter.inc' file. An example of a simplified parameter file is provided in Table A2. For this example the study area is defined by 4 columns and 5 rows, the maximum number of subdivisions per cell is 2, there are 4 soil texture classes, the number of attributes per subsection is 4 and the number of values for the Gaussian distribution is 100.

Table A1. Summary of data required for WE_DUST_EM

Data Type	Model Parameter	Description
Wind	10m wind speeds	Gridded 10m wind speed; input for WE_DUST_EM (wind.dat)
	Shear velocity (u_*)	Derived from 10m wind speeds using Prandtl -von Kármán equation; Calculated in WE_DUST_EM
Landcover	Surface soil texture	Generated using GIS; input for DUST_EM (surface_att.dat)
	Surface roughness length (z_0)	Derived from met. tower data (2010); input for WE_DUST_EM
Threshold shear velocity	Threshold shear velocity of soil (u_{*tsoil})	Minimum, mean and standard deviation for each surface soil texture class; input for WE_ DUST_EM
	Minimum threshold shear velocity (u_{*min})	Minimum threshold shear velocity for study site; input for WE_ DUST_EM
Dust Flux	Constants and exponents in power function	Power function where F is proportional to u_* for each soil texture class; input for WE_ DUST_EM

Table A2. Example of a parameter.inc

Input variables where (I) requires an Integer value (R) a Real number value and (T) Text input

Number of days (I): 1

Number of hours per day (I): 3

Number of columns for study area (I): 4

Number of rows for study area (I): 5

Number of soil texture classes (I): 4

Soil 1 (T): LS

Soil 2 (T): S

Soil 3 (T): SL

Soil 4 (T): SiL

Maximum subsections per grid cell (I): 2

Number of attributes per subsection (I): 4

Number of threshold shear velocity values in Gaussian distribution (I): 100

Minimum threshold shear velocity m/s (R): 0.17

Minimum threshold shear velocity m/s Soil 1 (R): 0.20

Minimum threshold shear velocity m/s Soil 2 (R): 0.17

Minimum threshold shear velocity m/s Soil 3 (R): 0.23

Minimum threshold shear velocity m/s Soil 4 (R): 0.25

Mean threshold shear velocity m/s Soil 1 (R): 0.45

Mean threshold shear velocity m/s Soil 2 (R): 0.30

Mean threshold shear velocity m/s Soil 3 (R): 0.32

Mean threshold shear velocity m/s Soil 4 (R): 0.34

STDev threshold shear velocity m/s Soil 1 (R): 0.63

STDev threshold shear velocity m/s Soil 2 (R): 0.04

STDev threshold shear velocity m/s Soil 3 (R): 0.04

STDev threshold shear velocity m/s Soil 4 (R): 0.05

Constant in power relationship for Soil 1 (I): 19486

Constant in power relationship for Soil 2 (I): 82501

Constant in power relationship for Soil 3 (I): 16528

Constant in power relationship for Soil 4 (I): 86

Exponent in power relationship for Soil 1 (R): 4.41

Exponent in power relationship for Soil 2 (R): 4.72

Exponent in power relationship for Soil 3 (R): 3.93

Exponent in power relationship for Soil 4 (R): 1.54

Two input files are needed to run the model, 1) the wind.dat file with 10m wind speeds and 2) the surface_att.dat with the attributes of each grid cell. An example of each input file for the study area defined above is provided in Tables A3 and A4. For each modelled hour, a value for the 10m wind speed is required for each grid cell in the format shown in Table A3.

Table A3. Example of a wind.dat input file

Hour	1		
3.47	4.19	3.66	5.05
2.48	3.76	6.14	5.45
3.37	4.06	2.58	4.76
4.16	3.81	2.38	3.86
1.95	3.07	5.08	4.47
Hour	2		
3.82	4.61	4.03	5.55
2.72	4.14	6.75	5.99
3.70	4.46	2.84	5.24
4.57	4.19	2.61	4.25
2.15	3.38	5.59	4.92
Hour	3		
5.79	6.98	6.11	8.42
4.13	6.27	10.23	9.08
5.61	6.77	4.31	7.94
6.93	6.35	3.96	6.44
3.25	5.12	8.46	7.46

The first two columns in the surface_att.dat file (Table A3) are filled with the coordinates of the centre of the model grid cell. The integer numeric code assigned to a soil texture fills the next column, for this example the numbers are as follows: 1=LS, 2=S, 3=SL, and SiL=4. The numeric code of 99 indicates the portion of the model grid cell outside of the study area. This numeric code can also be used to signify parts of the study area that are not of interest as they will not erode or emit dust, e.g. paved surfaces, water bodies, and forested areas. The percent coverage within the grid cell of each soil texture fills the next column. The surface roughness for that part of the grid cell fills the next column. Finally, the amount of that part of the model grid cell, which is bare erodible soil, fills the last column describing the surface attributes of that section of the grid cell. If the model grid cells have been subdivided, the parameter data for the remaining subareas of the cell are filled in the same manner. Once 100% of the grid cell has been parameterized, any remaining columns in the surface_att.dat file are filled with 0s (see Table A4).

Table A4. Example of a surface_att.dat file

x_coord	y_coord	soilnum1	%cover1	z01	% bare1	soilnum2	%cover2	z02	% bare2
-1680550	2179870	99	1	0	0	0	0	0	0
-1680490	2179870	2	1	0.002	1	0	0	0	0
-1680430	2179870	2	0.75	0.002	0.5	3	0.25	0.004	1
-1680370	2179870	3	0.5	0.004	0.25	2	0.5	0.002	1
-1680310	2179870	3	0.25	0.004	0.6	2	0.75	0.002	1
-1680250	2179870	3	0.3	0.004	1	2	0.7	0.002	0.25
-1680190	2179870	1	0.5	0.001	1	2	0.5	0.002	1
-1680130	2179870	2	0.25	0.002	0.1	2	0.75	0.002	1
-1680070	2179870	2	0.3	0.002	0.15	2	0.7	0.002	1
-1680010	2179870	1	0.75	0.001	1	2	0.25	0.002	1
-1679950	2179870	1	0.75	0.001	0.25	4	0.25	0.003	0.5
-1679890	2179870	1	0.5	0.001	1	3	0.5	0.004	1
-1679830	2179870	3	1	0.004	1	0	0	0	0
-1679770	2179870	2	1	0.002	1	0	0	0	0
-1679710	2179870	4	1	0.003	1	0	0	0	0
-1679650	2179870	4	1	0.003	1	0	0	0	0
-1679590	2179870	4	1	0.003	1	0	0	0	0
-1679530	2179870	4	0.5	0.003	1	99	0.5	0	0
-1679470	2179870	4	0.75	0.003	1	99	0.25	0	0
-1679410	2179870	99	1	0	0	0	0	0	0

Once the WE_DUST_EM code has been compiled with the parameter.inc file into an executable file for a study, all the wind.dat files, and the surface_att.dat have been assembled and formatted the modelling can be done. An example of the sequence of operations the WE_DUST_EM code carries out is provided in Fig. A1. This figure differs slightly from Fig. 1.3 in that it shows how multiple subareas within a model grid cell are handled, as the Williston beaches do not require multiple parts of a model grid cell Fig. 1.3 is a simplified version of Fig. A1.

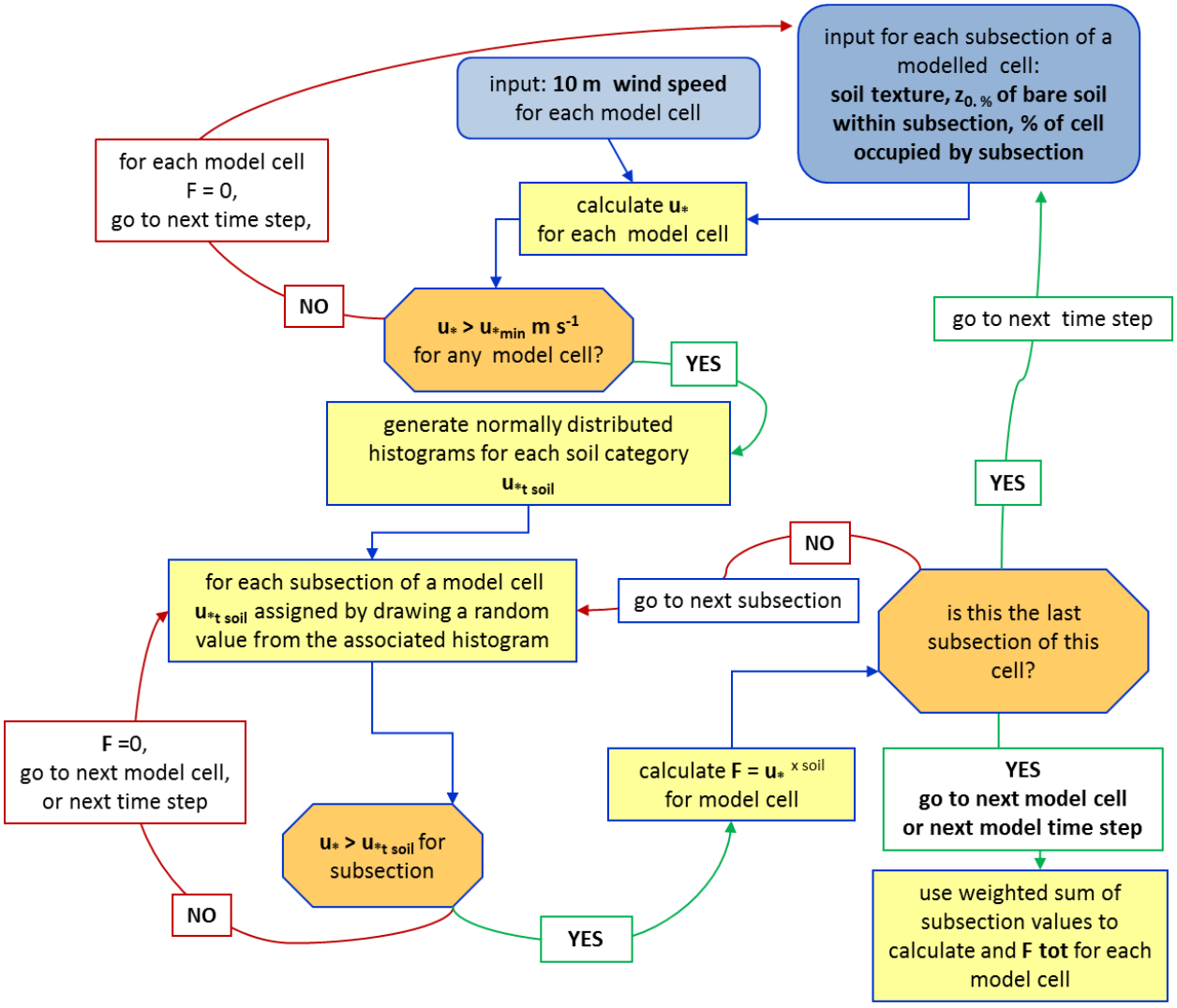

Figure A1. Computational flow of WE_DUST_EM.

The output files generated by WE_DUST_EM provide emissions data for each model grid cell by the hour. These data file can then be combined to produce daily dust emission totals which can then be imported into a GIS using the model cell coordinates to display the spatial pattern of wind erosion and dust emission sites.

GIS is used extensively not only to map the output data but also to build the surface_att.dat files. Future, plans for development of this model are to incorporate the code into a GIS system.